Modelling punching shear failure at edge slab-column connections by means of nonlinear joint elements

Deema Abu-Salma
PhD candidate, Department of Civil and Environmental Engineering, Imperial College London, London, United Kingdom

Robert L Vollum*
Professor of Structural Concrete, Department of Civil and Environmental Engineering, Imperial College London, London, United Kingdom

Lorenzo Macorini
Reader in Structural Engineering, Department of Civil and Environmental Engineering, Imperial College London, London, United Kingdom

*Corresponding author email: r.vollum@imperial.ac.uk

Abstract

This paper is concerned with the modelling of punching shear failure at edge columns of flat slabs without shear reinforcement. Punching failure at edge columns is much less researched than at interior columns despite typical buildings having more edge than interior columns. The paper uses nonlinear finite element analysis (NLFEA) to study the influence on punching resistance of parameters including column aspect ratio and loading eccentricity. The NLFEA is carried out using both 3D solid elements and a Joint Shell Punching Model (JSPM) which combines nonlinear shell elements with nonlinear joint elements that incorporate the failure criterion of the Critical Shear Crack Theory (CSCT). Both constant and varying loading eccentricities are investigated since near failure eccentricity at edge column connections typically reduces below that calculated with elastic analysis due to moment being redistributed from the support to span. This reduction in eccentricity is beneficial since punching resistance is shown to depend on the final loading eccentricity. Consequently, designing for punching on the basis of elastic edge column moments is overly conservative.

1. Introduction

Recent research into punching failure has been mainly directed towards isolated interior slab-column connections despite buildings typically having more exterior than interior columns. Furthermore, unlike interior columns, significant loading eccentricity cannot be avoided at perimeter columns which complicates their design. Despite this, current codified punching shear design provisions are largely based on detailed study of concentrically loaded isolated interior slab-column connections.

Punching failure is most realistically captured numerically using 3D solid elements, but this is highly computationally demanding. Conventional nonlinear shell elements are more efficient for modelling flexural behaviour but suffer from the disadvantage that shear failure is not captured. Two alternative approaches are reported in the literature for overcoming this problem. In the first approach [1, 2], a layered shell element is developed to account for the 3D state of stress and strain in each layer. To calculate the out-of-plane normal strain, the out-of-plane normal stress is assumed to be negligible. In the second approach, flexure is modelled with 2D shell elements while 3D nonlinear connector elements are placed around the column to simulate the separation of the column from the slab at punching failure [3-6].

The JSPM of Setiawan et al. [6] simulates punching failure by placing nonlinear joint elements around a control perimeter located at 0.5d from the column face, where d is the slab effective depth (see Figure 1). The joint elements are used to connect the shell elements located to either side of the critical control perimeter. Prior to joint shear failure, out of plane joint shear stiffness is taken as:

$$k_{inc} = k_{red} \cdot \frac{E_C}{2(1+v)} \cdot l_{si} \tag{1}$$

where v is Poisson's ratio which is taken as 0.2, E_c is the concrete elastic modulus, k_{red} is an out-of-plane stiffness reduction factor accounting for cracking and l_{si} is the spacing of joint i calculated with rounded corners to give the same total control perimeter as used in the CSCT. In [6], k_{red} is taken as 0.1 when modelling punching at isolated interior columns.

The punching resistance of each joint is calculated in accordance with the CSCT of Muttoni [7] as follows:

$$V_{ji} = \frac{3/4\sqrt{f_c}}{1 + 15\frac{\psi_{si} \cdot d}{16 + d_g}} l_{si} d \tag{2}$$

where V_{ji} is the shear resistance of joint i, f_c is the concrete cylinder strength, ψ_{si}, is the relative slab column sector rotation of joint i which is continuously updated throughout the analysis, d_g is the maximum aggregate size and d is the average slab effective depth. Subsequent to shear failure, the joint shear force is given by equation 2. The slab rotation is extracted for each sector along the line of radial contraflexure as indicated in Figure 1. Further details are given in [6].

This paper extends the JSPM of Setiawan et al. [6] to the analysis of punching failure at edge columns of flat slabs. The modified JSPM, depicted JSPME in which 'E' stands for edge columns, is shown to be capable of accurately simulating punching shear failure of both isolated and continuous edge slab-column connections with varying loading eccentricity, column aspect ratio and slab edge boundary conditions.

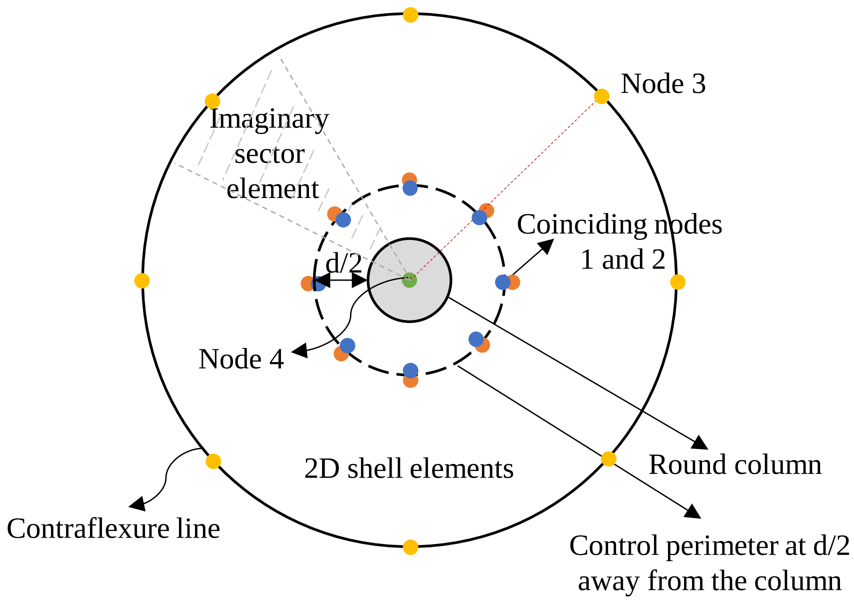

Figure 1: JSPM for interior column-slab connections

2. Nonlinear finite element analysis with 3D solid elements

In addition to laboratory test data, the JSPME is validated using virtual slab-column specimens simulated with NLFEA using 3D solid elements. The solid element analysis was carried out with ATENA [8] using the procedure of Setiawan et al. [6,9,10] who in [6] analysed punching failure of 16 slabs without shear reinforcement having either square supports (14) or elongated supports (3). The resulting mean value of $P_{test}/P_{predicted}$ was 0.95 with a coefficient of variation of 7.3%. Concrete was modelled using CC3DNonLinCementitious2 [8] which is a fracture-plastic model combining constitutive models for concrete in tension as well as compression. Based on calibration studies, a fully rotating crack model was used. Compressive fracture of concrete in CC3DNonLinCementitious2 is related to a critical compressive displacement, w_d, which based on calibration studies was taken as 0.5 mm. The concrete compressive strength was reduced parallel to the crack direction, similarly to the Modified Compression Field Theory [11]. The strength reduction is related to the largest maximal fracturing strain and is limited to a ratio r_c of the uniaxial concrete compressive strength. Concrete members were meshed using linear order hexahedra elements, while steel loading plates were meshed using linear order tetrahedra elements. Reinforcement was modelled with a bilinear stress-strain relationship assuming perfect bond. The slabs were loaded using force-control in conjunction with the arc-length method. A convergence criterion of 1% was assigned for the displacement, residual force and absolute residual force error while a 0.01% criterion was assigned for the energy error. Table 1 summarises the material properties and input parameters used in the ATENA analyses of this paper which are the same as used previously in [6,9].

Table 1: Summary of material parameters and numerical input for NLFEA in ATENA.

No.	Parameter	Value/Reference
	Concrete constitutive model	
A1	Concrete elastic modulus	Model Code 2010 [12]
A2	Fracture energy	Model Code 2010 [12]
A3	Concrete tensile strength	Model Code 2010 [12]
A4	Smeared crack model	Fully-rotating crack
A5	Critical compressive displacement w_d	0.5 mm
A6	Limit of compressive strength reduction due to cracking (MCFT)	$0.8f_c'$
A7	Eccentricity (defining the shape of the failure surface)	0.52
A8	Volume dilatation plastic factor	0
	Reinforcement bar model	
B1	Stress-strain relationship	Bilinear with strain hardening modulus of 0.2 MPa
B2	Bond-slip model	Perfect bond
	Loading procedure and convergence criteria	
C1	Loading procedure	Static (force-controlled)
C2	Solution procedure	Arc-length method
C3	Convergence criteria for displacement, residual force, and absolute residual force error	1%
C4	Convergence criterion for energy error	0.01%
	Mesh properties	
D1	Mesh size (finest)	m x m x m mm (10 elements along height)
D2	Mesh element for concrete slab	8-noded hexahedral (linear)
D3	Mesh element for loading apparatus	4-noded tetrahedral (linear)
D4	Mesh element for reinforcement bar	2-noded truss element (embedded)

2.1. Validation of 3D solid element modelling

Use of the ATENA modelling parameters proposed by Setiawan et al. [9] was validated in this study by modelling the four internal and 11 external punching specimens listed in Table 2. All the edge column specimens listed in Table 2 were also modelled using the JSPME. Slabs L1, L2, L5 and L6 of Albuquerque et al. [13] measured 2350 mm long, 1700 mm wide and 180 mm thick with an average effective depth of 147 mm (see Figure 2). The slab was supported at one end by a 300 mm square column and at the other end by a fixed full width roller support. Loading eccentricity was imposed through a boot located at the base of the column. The unsupported slab edges were loaded by four equal point loads. Slabs HXXX and XXX of EL-Salakawy et al. [14] measured 1540 mm long, 1020 mm wide and 120 mm thick. The average effective depth was 88.75 mm. The column was 250 mm square and positioned at the centre of the free edge with its outside face flush with the slab edge. The other slab edges were simply supported on stiff supports. The column was loaded with combined vertical and horizontal loads to provide a constant inward eccentricity relative to the column centreline of 300 mm and 660 mm in slabs XXX and HXXX respectively.

Specimens 1, 2 and 4 of Regan [15] had a 300 mm square column positioned at the centre of each short edge of the slab which measured 5784 mm long, 3000 mm wide and 200 mm thick. The longitudinal flexural tension reinforcement ratio in the span was 0.5%. The flexural tension reinforcement normal to the slab edge was provided with U bars having a reinforcement ratio ρ_{sup}, within a width of 900 mm centred on the column, of 0.8% in slabs S1 to S3, 1.0% in S4 end 1 and 0.5% in S4 end 2. The two ends of each slab were tested separately, with the column providing the support at one end. The other end was simply supported on a full width roller positioned just inside the column face. The slabs were loaded with evenly spaced point loads along their long edge. Further details can be found in [15,16].

Table 2: Flat slab-column connections modelled with ATENA Cervenka et al. [8].

Slab	Source	Column location	Specimen type	Column size (mm^2)	Slab thickness h (mm)	f_c (MPa)	Maximum aggregate size (mm)	V_{TEST}/V_{ATENA}
PT22*	[17]	Interior	Isolated	260 x 260	250	67	16	989/1012= 0.98
PT31*						66.3		1433/1489= 0.96
OC13*	[18]	Interior	Isolated	200 x 600	150	35.8	20	568/573.5 = 0.99
LS06**	[19]	Interior	Isolated	300 x 300	180	50	9.5	582/501 = 1.16
XXX**	[14]	Edge	Isolated	250 x 250	120	33	15	125/118 = 1.06
HXXX**					120	36.5		69/61= 1.13
L1**	[13]	Edge	Isolated	300 x 300	180	46.8	9.5	308/345 = 0.89
L2*						44.7		315/318= 0.99
L5$^+$						51.4		374/415 = 0.90
L6$^+$						52.1		330/344 = 0.96
Slab 1 end 1**	[15]	Edge	Continuous	300 x 300	200	35.4	20	282/252 = 1.12
Slab 1 end 2**						35.4		264/252 = 1.05
Slab 2 end 1**						35.4		256/259 = 0.99
Slab 2 end 2**						35.4		285/263 = 1.08
Slab 4 end 1**						42.7		289/270 = 1.07
Slab 4 end 2**						42.7		281/260 = 1.08
						Mean		1.02
						Standard deviation		0.08

*Note: * concentric loading, ** eccentric loading, + outward eccentricity.*

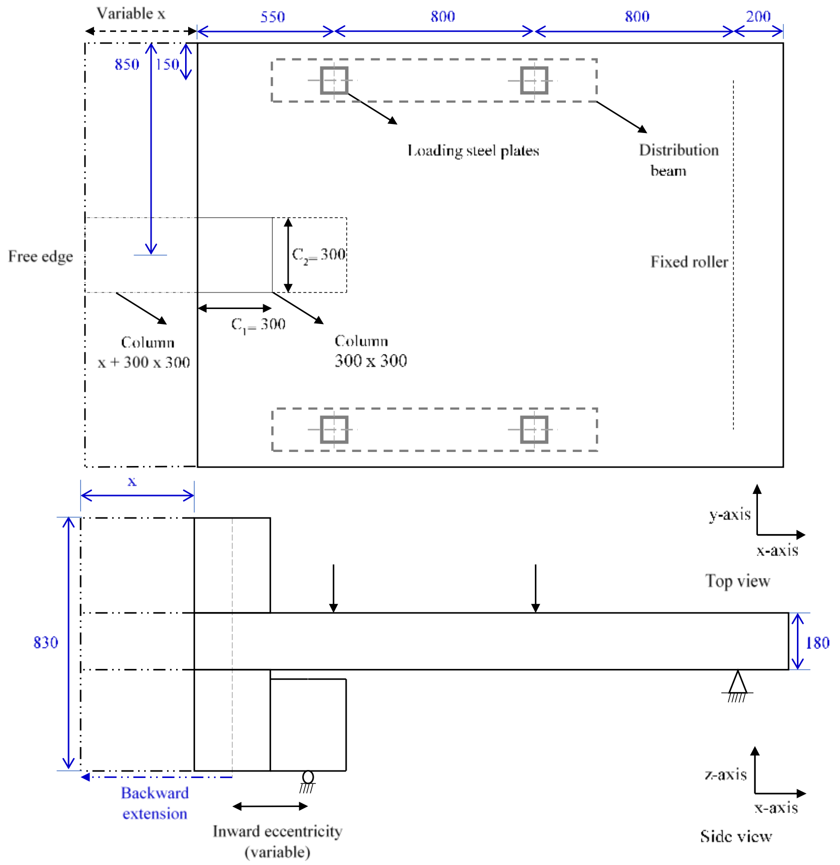

Figure 2: Plan showing original and parametric test set-up regenerated from Albuquerque at al. [13] (all dimensions in mm).

2.2 Mesh sensitivity study and strain based failure criterion

A mesh sensitivity study was undertaken using slabs HXXX and XXX [14]. The study considered the use of uniform meshes with either five or seven hexahedral-linear elements through the slab thickness and a gradated mesh (see Figure 3) similar to that used by Setiawan et al. [9]. In the latter approach cubic elements with side length $m = h/10$ (where h is the slab thickness) were used to model the slab within a distance of 2d from the column face. A coarser mesh, on plan, with element sides measuring $2m \times m \times m$ (i.e. length × width × thickness), $m \times 2m \times m$, or $2m \times 2m \times m$ was used elsewhere. Figure 4 compares the load deflection responses obtained using all three meshes. The effect of refining the mesh is seen to be more pronounced for slab HXXX than slab XXX with the gradated mesh giving the best overall results. Consequently, the gradated mesh was adopted in the analyses presented in this paper as illustrated in Figures 3 and 5 for the slabs of [14] and [15] respectively. Figure 4 also shows the load deflection responses obtained by Genikomsou and Polak [20] using ABAQUS [21]. Like the ATENA responses, the ABAQUS response of [20] is also overly stiff for HXXX.

As found by Setiawan et al. [10], a distinct softening branch was not always captured in the ATENA analyses. Consequently, the strain based failure criterion of Setiawan et al. [10] was adopted. This criterion is based on the experimental observation (e.g. Ferreira et al. [22]) that radial strain in the slab soffit drops to zero near the column face at or near the peak punching shear load. A similar strain based failure criterion was adopted by Broms [23] in his analytical model for punching failure. In the present work, punching failure is assumed to occur at the lower of the peak load obtained in the NLFEA and that at which the radial compressive strain in the slab soffit first drops to zero at a distance of 0.5d from the column face. Failure loads obtained using the strain criterion are plotted in Figure 4 for specimens XXX and HXXX and Figure 6 for specimen L2 of Albuquerque et al. [13]. In all cases, the failure loads obtained using the strain criterion are similar to the corresponding peak load obtained with ATENA, thereby justifying use of the strain criterion. The statistics in Table 2 show that use of the adopted modelling procedure gives good estimates of punching resistance for the considered test specimens.

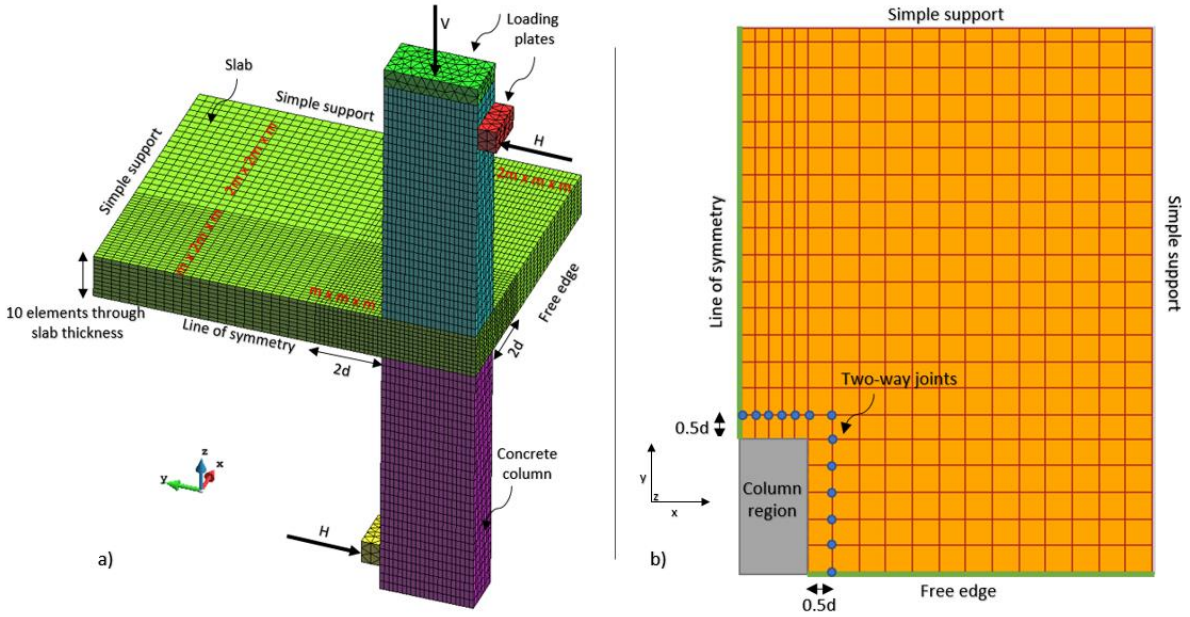

Figure 3: Mesh configuration and boundary conditions for slab XXX in a) ATENA and b) the JSPME in ADAPTIC

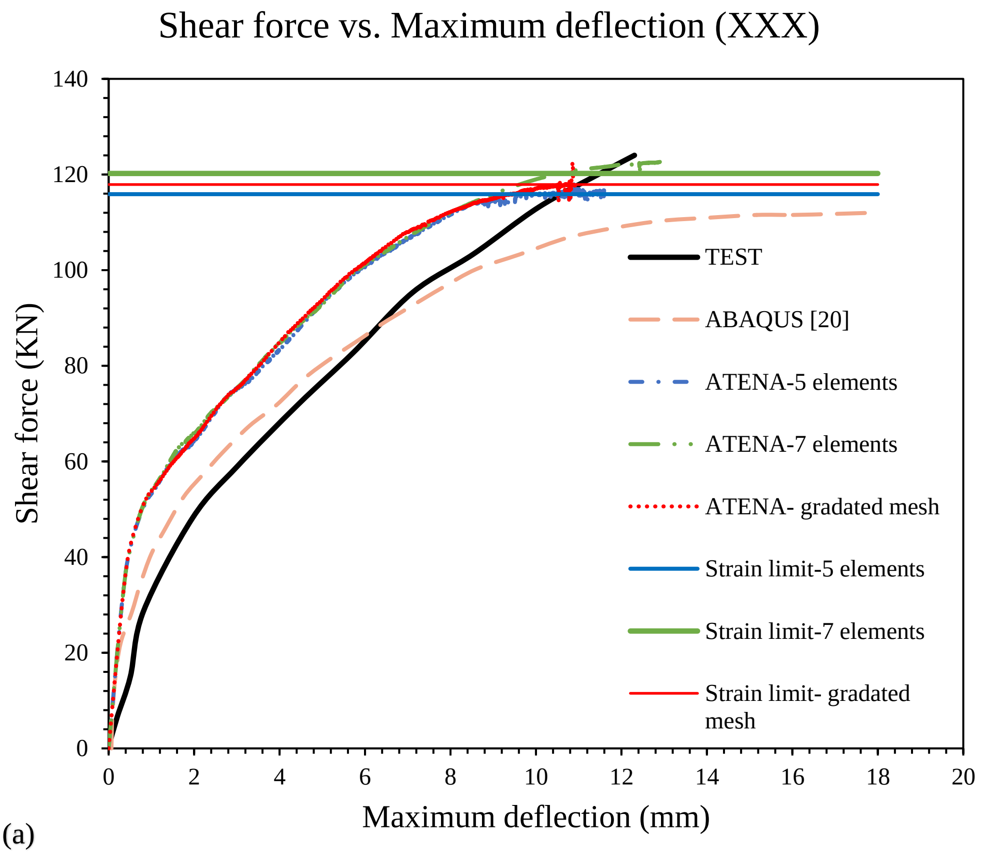

(a)

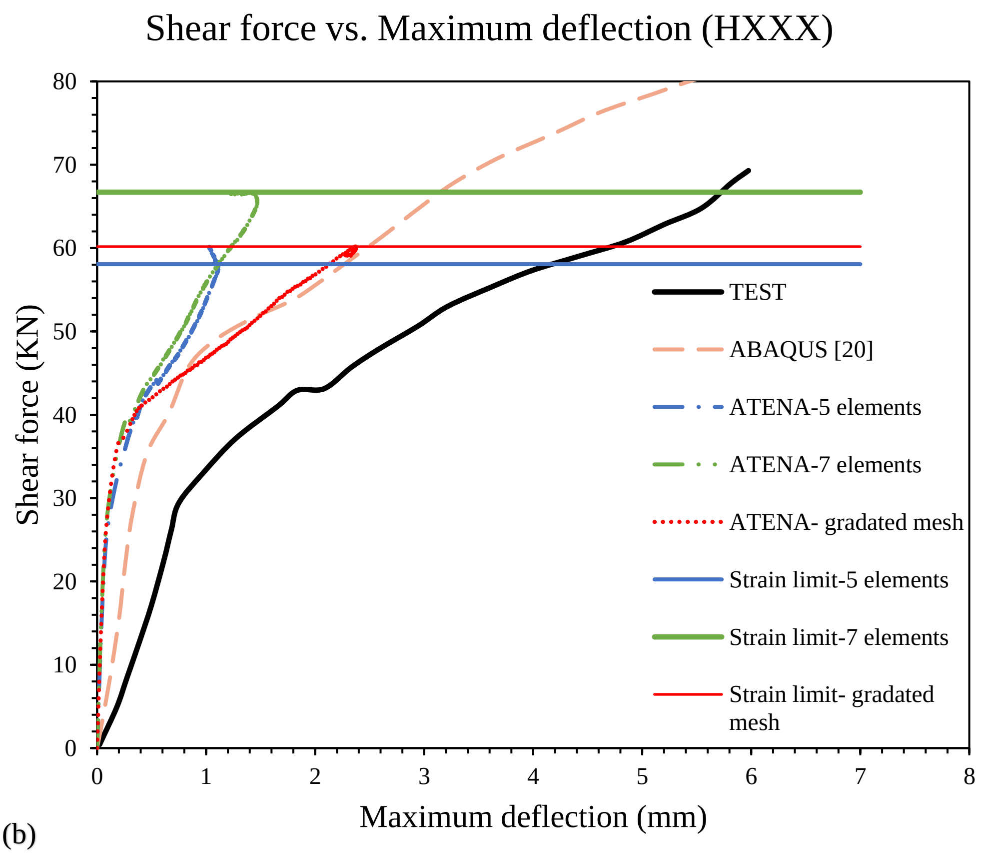

(b)

Figure 4: Mesh sensitivity analyses in slabs a) XXX [14] and b) HXXX [14]

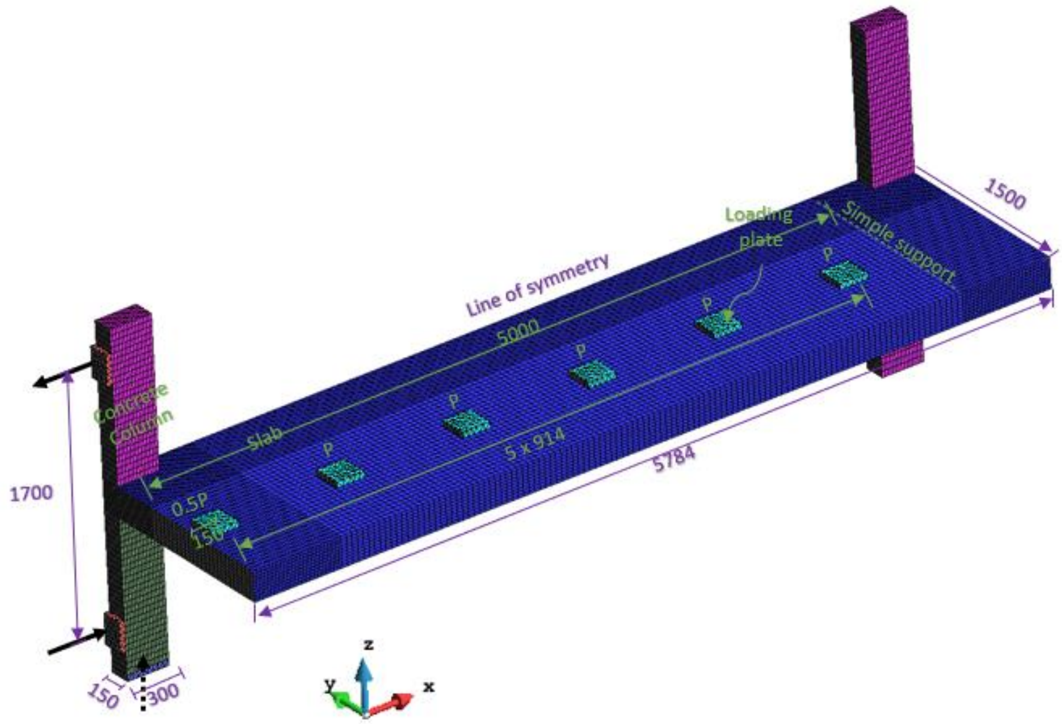

Figure 5: Mesh configuration and boundary conditions for Regan [15] slabs in ATENA

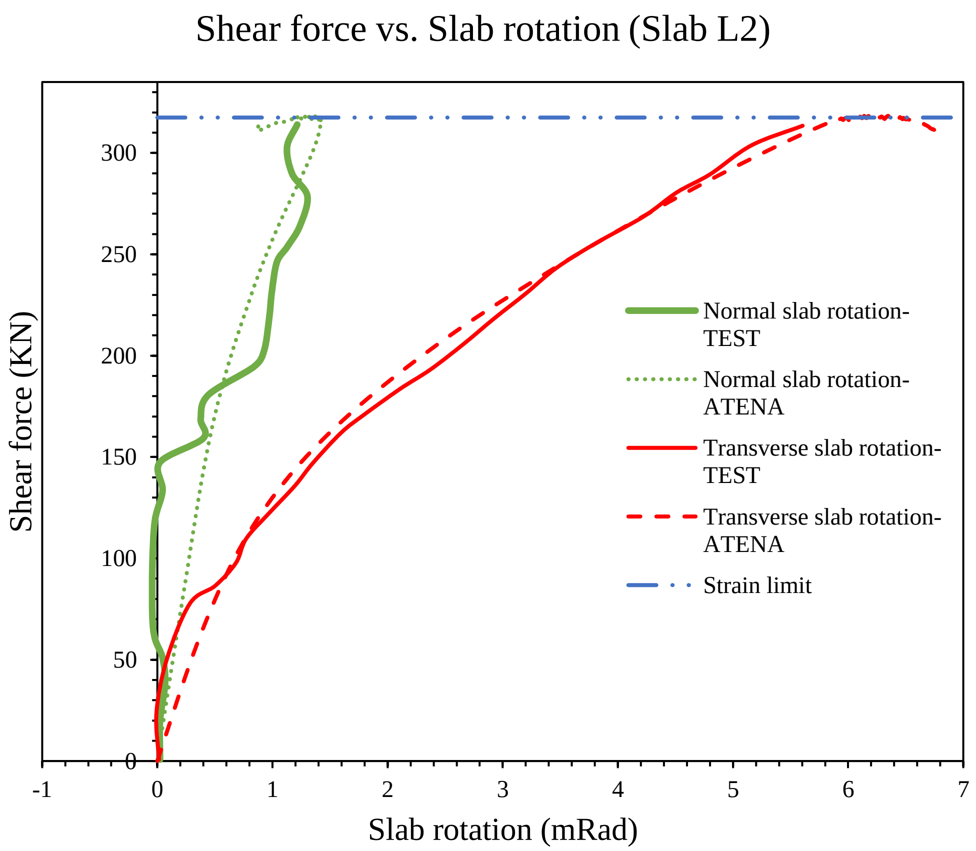

Figure 6: Strain criterion evaluation in slab L2 [13]

3. NLFEA parametric study of column aspect ratio

Punching failure has hardly been studied at elongated edge columns despite them being commonly used to provide vertical support within non-load bearing partitions of residential buildings. Consequently, there is an almost complete lack of experimental data to assess punching resistance at elongated edge columns. In the absence of experimental data, this paper uses NLFEA, with 3D solid elements to investigate the influence of edge column elongation on punching failure at edge columns.

3.1. Full-scale flat-slab frame building analysed in ETABS

The range of considered loading eccentricities is based on a parametric study of a full-scale flat-slab frame building with varying spans and column aspect ratios. The analysed floor slab had two bays in both the longitudinal and the transverse directions with floor-to-floor height of 3 m. The spans were varied independently in each direction between 4 m and 9 m. The slab thickness for each span length combination was derived using charts given in Economic Concrete Frame Elements to Eurocode 2 [25]. For each combination of spans considered, the perimeter column size was taken as 300 mm x 300 mm, 600 mm x 300 mm, 750 mm x 300 mm and 1000 mm x 300 mm with the longer column side perpendicular to the slab edge. The slab was modelled in ETABS using elastic shell-thick elements that were connected to linear column elements via rigid links. The slab was loaded with characteristic dead and imposed loads of 1.5 kN/m^2 and 3.0 kN/m^2 respectively. EC2 load factors of 1.35 for dead load and 1.5 for imposed load were used. Analyses were undertaken with and without a cladding load of 10 kN/m around the building perimeter. Pattern loading was considered for analyses with cladding load included. The minimum eccentricities in Table 3 correspond to uniform loading with cladding. Maximum eccentricities in Table 3 correspond to uniform loading without cladding which were slightly greater than pattern loading with cladding. The resulting eccentricities are considered indicative of those likely to arise in practice, but actual eccentricity depends on the adopted structural arrangement and loading. The loading eccentricity ($e = M_{col}/V$ where M_{col} and V depict the moment and shear force transferred to the edge column) was calculated for each considered structural arrangement, thereby, giving a practical range of eccentricities for elongated edge columns. Table 3 below summarises the obtained range of eccentricities, relative to the column centreline, for each column size. By way of reference, for fully fixed supports, $M_{col}/V= 0.16L$ for uniformly distributed loading where L is the span length.

Table 3: Full-scale flat-slab frame structure results

Column size (mm x mm)	Range of developed eccentricities about column centreline (mm)	Range of developed eccentricities as proportion of span
300 x 300	256-520	$\frac{256}{6000} - \frac{294}{4000} = 0.042 - 0.073$
600 x 300	319-971	$\frac{319}{4000} - \frac{489}{4000} = 0.080 - 0.122$
750 x 300	326-1160	$\frac{326}{4000} - \frac{522}{4000} = 0.082 - 0.130$
1000 x 300	313-1236	$\frac{313}{4000} - \frac{816}{6000} = 0.078 - 0.136$

3.2. Parametric study of elongated edge columns

Specimens with geometry based on slab L1 of Albuquerque et al. [13] and slab XXX of El-Salakawy et al. [14] were considered in the parametric study. The column and the slab edge of both specimens were extended backwards as shown in Figure 2 for slab L1 where the dimensions c_1 and c_2 refer to the long and short column sides respectively. The loading eccentricity was varied by adjusting the position of the roller at the boot of the column. No other changes to the tested geometries were made. The concrete and reinforcement properties used in the parametric study were the same as used in modelling the original specimens, but the reinforcement bar diameter was increased where necessary to avoid flexural failure. A range of loading eccentricities, based on Table 3, was investigated for each column size as shown in Table 4 below. The specimen type and the loading eccentricity magnitude are indicated in the slab designation. For example, the notation L1-300 indicates specimen type, L1 and loading eccentricity of 300 mm. The strength and load deformation responses of the specimens were obtained using 3D solid element modelling with ATENA. The shear force distributions around a rectangular perimeter at 0.5d from the column face were also extracted to give insight into the failure mechanism. Presentation and discussion of the results of the parametric study is delayed until section 4 where results obtained using 3D solid element modelling and the JSPME are compared. The concrete strengths in Table 4 are the same as reported for the test series from which the specimens are derived.

Table 4: Summary of virtual slabs used in parametric study

Slab	Column dimensions (mm x mm)	M_{col}/V (mm)	h (mm)	d (mm)	f_c (MPa)	f_{ct} (MPa)	E_c (GPa)
L1	300 x 300	300, 500, 700	180	147	46.8	3.4	29.3
L1a	600 x 300	500, 700, 1000	180	147	46.8	3.4	29.3
L1b	750 x 300	500, 700, 900, 1200	180	147	46.8	3.4	29.3
L1c	1000 x 300	600, 800, 1000, 1200	180	147	46.8	3.4	29.3
XXX 250 x 250	250 x 250	203, 230, 327, 394, 431, 486, 504, 605	120	88.75	33	3.38	MC2010 [12]
XXX 500 x 250	500 x 250	500, 700, 800, 900	120	88.75	33	3.38	MC2010 [12]

4. Implementation of the JSPM into ADAPTIC

The JSPM is implemented in the NLFEA program ADAPTIC [26] where the slab is modelled with 2D nonlinear shell elements. The adopted nonlinear shell element utilises the Reissner-Mindlin hypothesis and accounts for in plane material and geometric nonlinearities. A linear out-of-plane shear response is adopted. In this study, the shell elements are discretised into 10 in-plane layers through the slab thickness. Concrete compressive behaviour is modelled using a plasticity approach in which compressive stress is determined from an evolving plastic interaction surface in the biaxial plane. Concrete tensile behaviour is formulated independently using a smeared fixed-crack approach in which the crack direction is determined from the principal stress direction at the moment of first cracking. Following cracking, the in-plane shear stiffness is reduced by a constant shear retention factor (β_s) which was taken as 0.1 in this study. However, this choice has no significant effect on the predicted load rotation response, and hence the JSPME failure load, as previously shown by Soares [27]. Reinforcement is modelled with equivalent uniaxial plates of uniform thickness assuming perfect bond and a bilinear stress-strain curve (with minimal strain hardening). In this study, the concrete elastic modulus (E_c) and concrete tensile strength (f_t) were determined using Model Code 2010 [12] for consistency with the input parameters adopted in ATENA (see Table 1). As suggested by Vollum and Tay [28], the concrete tensile strength was reduced by a factor of two in ADAPTIC, and the tensile softening slope was chosen to reduce tensile stress to zero at a strain of 0.001. This approach gives reasonable estimates of slab deflection as illustrated in this paper and elsewhere [6]. The slab shell elements are connected via rigid links to the columns which are modelled using linear elements. As explained by Setiawan et al. [6], the joints of the JSPME are modelled with the jel 3 element in ADAPTIC which has 4 nodes of which nodes 1 and 2 are initially coincident and positioned around the punching control perimeter (see Figure 3b). The x-axis and the plane in which the y-axis is positioned are defined by nodes 3 and 4 respectively. Node 3 is located in the same sector as nodes 1 and 2 at the position where the relative slab-column rotation is greatest. Typically, rotations are greatest near the line of elastic radial contraflexure. Node 4 is located on the column chord immediately above the slab. The shear resistance of each joint is calculated at each load step in terms of maximum relative slab-column rotation in its sector which is given by the difference between the rotations at nodes 3 and 4 (see Figure 1).

4.1 Extension of JSPM to punching at edge columns

Without an additional failure criterion, the JSPM overestimates punching shear resistance at edge columns since global failure is triggered by failure of all the joints around the control perimeter. As a consequence, it is necessary to trigger punching failure before all joints fail as done in [6] for eccentrically loaded internal slab-column connections. Based on numerical simulations of the laboratory tested edge connections listed in Table 2, for column sides with length less than 3d, global failure is assumed to take place when the joint located at the centre of side c_1 fails (see figure 7a). For column sides with length greater than 3d, the reduced control perimeter of fib Model Code 2010 [12] shown in Figure 7b is used in the JSPM. Dummy joints having minimal shear resistance are placed along the neglected portion of the control perimeter. Global failure is assumed to occur when the two-way joints located on sides c_1 at 1.5d from the inner column end fail.

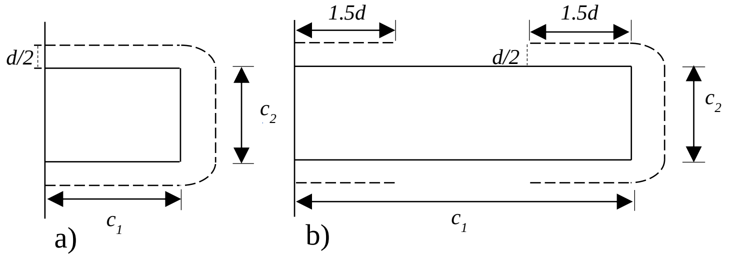

Figure 7: Control perimeter by MC2010 with a) c_1 and c_2 < 3d (b_0) and b) c_1 > 3d and c_2 < 3d ($b_{0,3d}$)

4.1.1 Introduction of torsional limit on joint strength

The JSPM load-rotation response and failure load depend not only on the location of the joint at which global failure is triggered but also on the joint torsional strength and shear stiffness, k_{inc} (see equation 1). Parametric studies show that for both edge and internal [6] slab column connections, reducing k_{inc} increases punching resistance but has virtually no influence on the load deflection response. Physically, reducing k_{inc} reduces the proportion of unbalanced moment resisted by eccentric shear relative to flexure and torsion. This in turn reduces the joint shear forces at given unbalanced moment, thereby, increasing punching resistance. Setiawan et al. [6] adopted k_{red} = 0.1 for internal slab column connections but this was found to overestimate the strength of edge column connections, where taking k_{inc} = 1e12 N/mm gives better predictions of failure load as well as joint shear force. The reason for this difference appears to that redistribution of shear forces around the control perimeter is more pronounced in internal than external connections. In the latter, behaviour is more influenced by moment transfer to the column sides perpendicular to the slab edge through torsion. This is accounted for in the JSPME by limiting the torsional resistance of the joint elements. A rigid-plastic torsional response is assumed for the joint elements. The joint torsional resistance of joint i, T_{cri}, is determined as follows in accordance with the recommendations of Hsu [29] as done in the macro-model of Liu et al. [4,5] for punching at internal slab column connections.

$$T_{cri} = 0.217 l_{si}(h^2 + 6450)\sqrt[3]{f_c'} \quad (3)$$

in which l_{si} and h (mm) are the joint spacing and slab thickness respectively and f_c' is the concrete compressive strength (MPa). The JSPM with joint torsional resistance limited to T_{cri} is depicted JSPME.

4.1.2 Assessment of JSPME load displacement response

Measured and predicted load displacement responses are compared in Figure 8 for specimens a) XXX and b) HXXX of EL-Salakawy et al. [14], c) L2 of Albuquerque et al. [13], d) L1-500, e) L1-700 and f) L1b-700 from Table 4. JSPM results are shown without (JSPM) and with (JSPME) the joint torsional strength limited to T_{cri} for k_{inc} 1e12 N/mm. The introduction of joint elements significantly softens the load rotation response as shown in Figures 8d and 8e where the ADAPTIC load rotation response without joint elements is also plotted. The limit on torsional strength only comes into play at large loading eccentricities as seen in Figures 8d to 8f where the ATENA response is better captured by the JSPME than the JSPM. Both the JSPME and ATENA capture the experimental load displacement response well for slabs XXX and L2 but less well for HXXX where the predicted response is overly stiff. Figure 9, which is representative, shows that the JSPME and ATENA load-rotation responses also compare well up to failure of the JSPME for virtual slab series XXX 500 x 250.

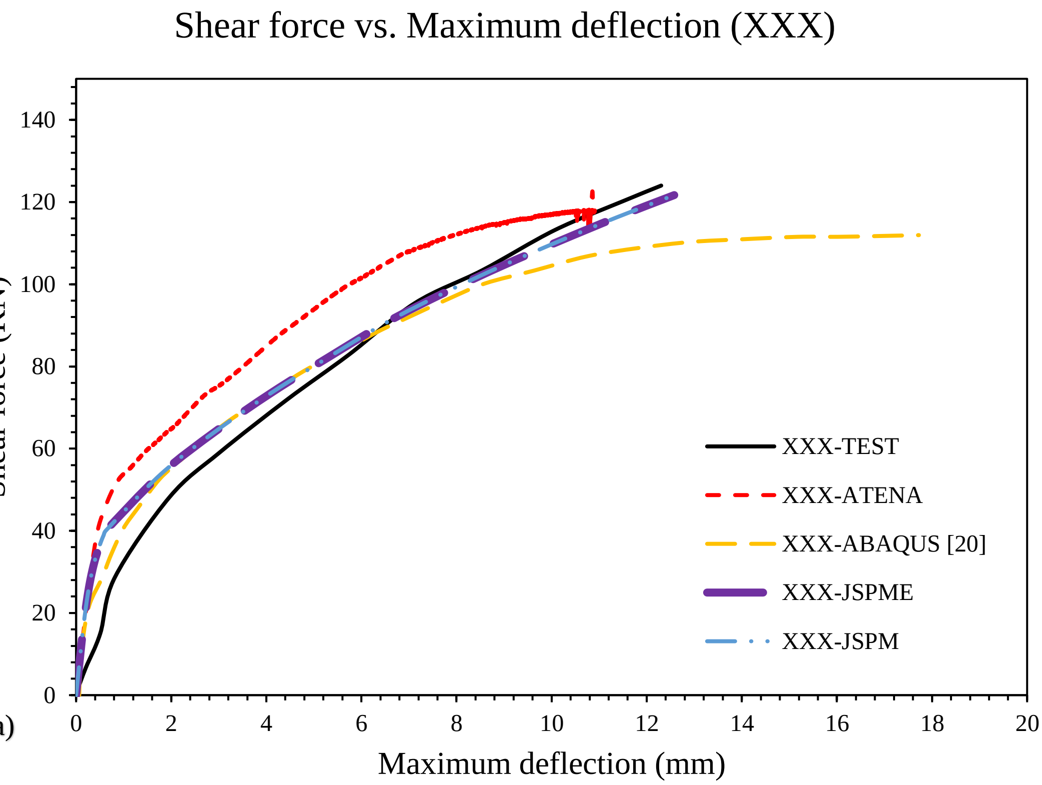
Shear force vs. Maximum deflection (XXX)
Shear force (KN)
0
20
40
60
80
100
120
140
0
2
4
6
8
10
12
14
16
18
20
Maximum deflection (mm)
XXX-TEST
XXX-ATENA
XXX-ABAQUS [20]
XXX-JSPME
XXX-JSPM

(a)

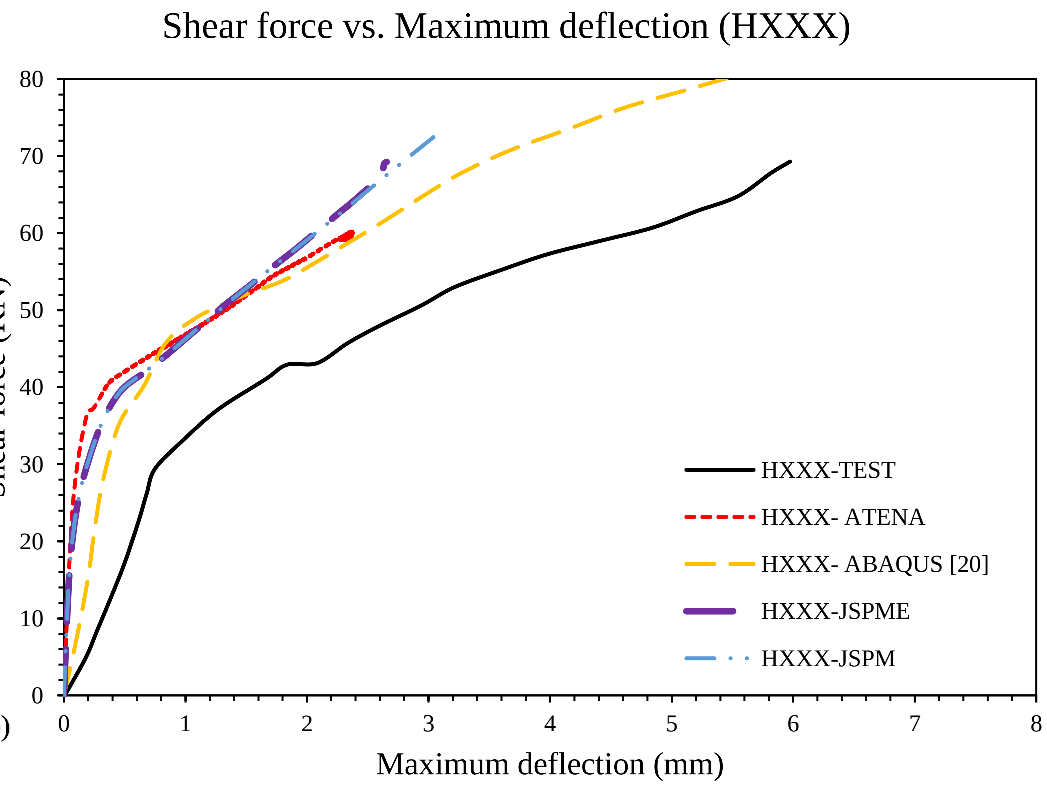
Shear force vs. Maximum deflection (HXXX)
Shear force (KN)
0
10
20
30
40
50
60
70
80
0
1
2
3
4
5
6
7
8
Maximum deflection (mm)
HXXX-TEST
HXXX- ATENA
HXXX- ABAQUS [20]
HXXX-JSPME
HXXX-JSPM

b)

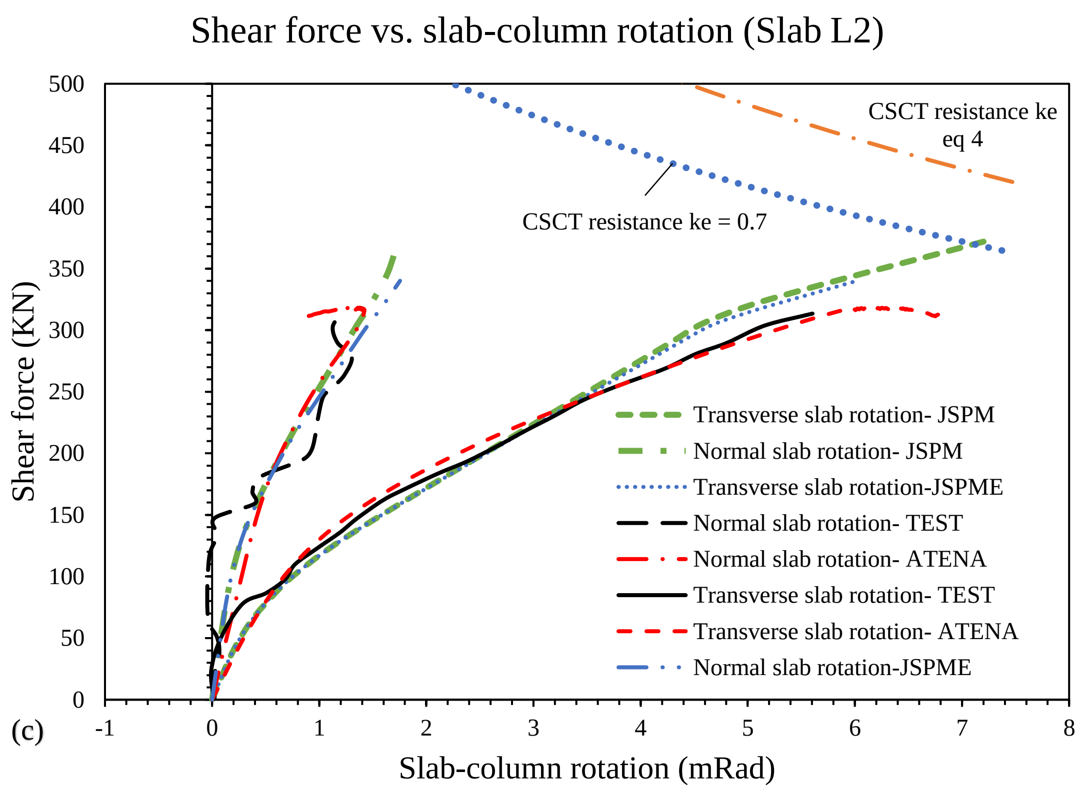
Shear force vs. slab-column rotation (Slab L2)
Shear force (KN)
Slab-column rotation (mRad)
CSCT resistance ke eq 4
CSCT resistance ke = 0.7
Transverse slab rotation- JSPM
Normal slab rotation- JSPM
Transverse slab rotation-JSPME
Normal slab rotation- TEST
Normal slab rotation- ATENA
Transverse slab rotation- TEST
Transverse slab rotation- ATENA
Normal slab rotation-JSPME

(c)

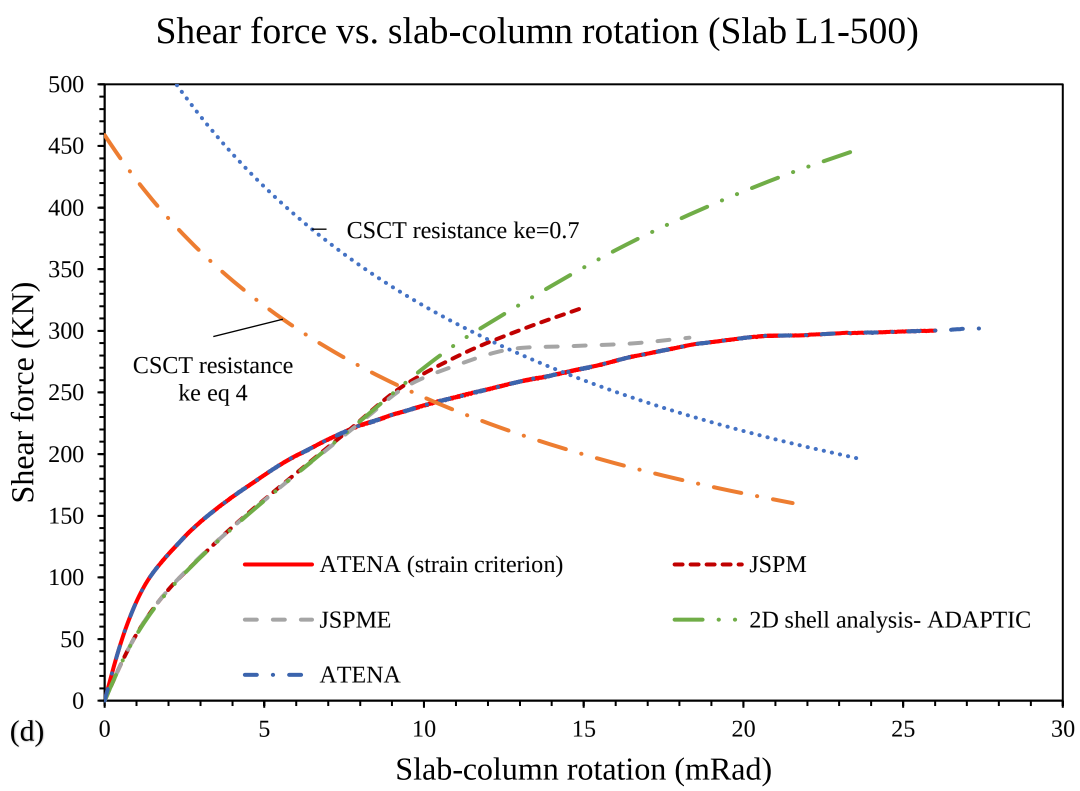
Shear force vs. slab-column rotation (Slab L1-500)
Shear force (KN)
Slab-column rotation (mRad)
CSCT resistance ke=0.7
CSCT resistance ke eq 4
ATENA (strain criterion)
JSPM
JSPME
2D shell analysis- ADAPTIC
ATENA

(d)

(e)

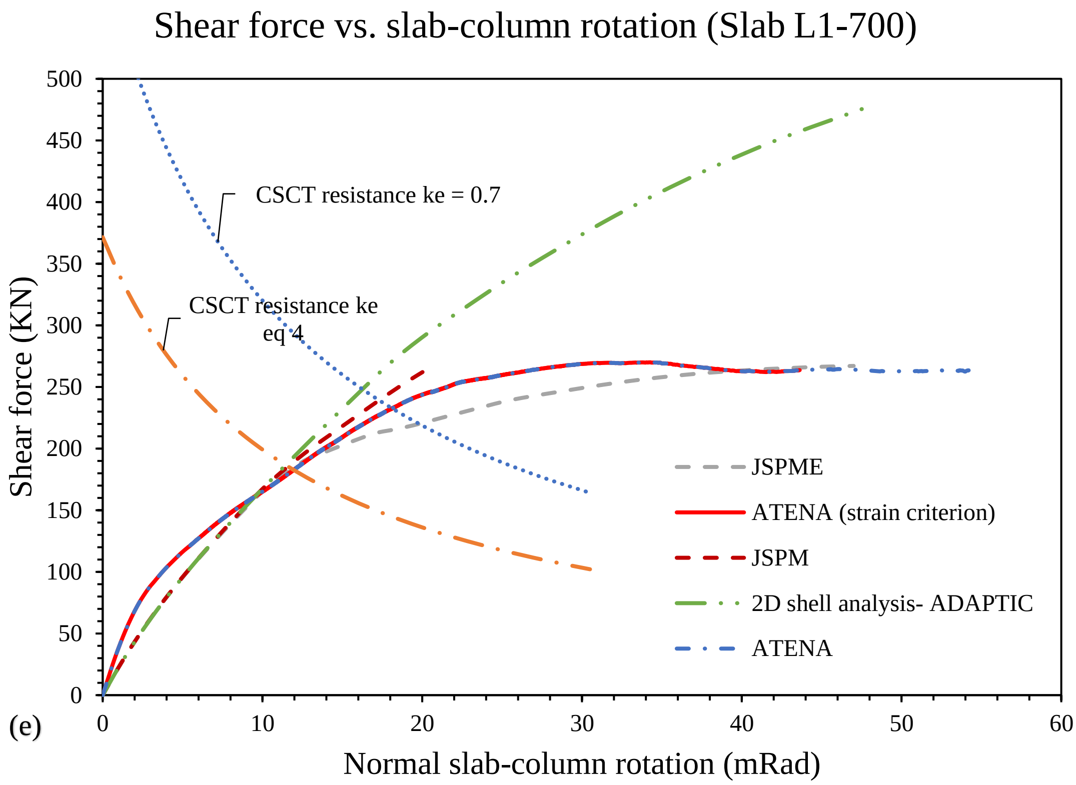

(f)

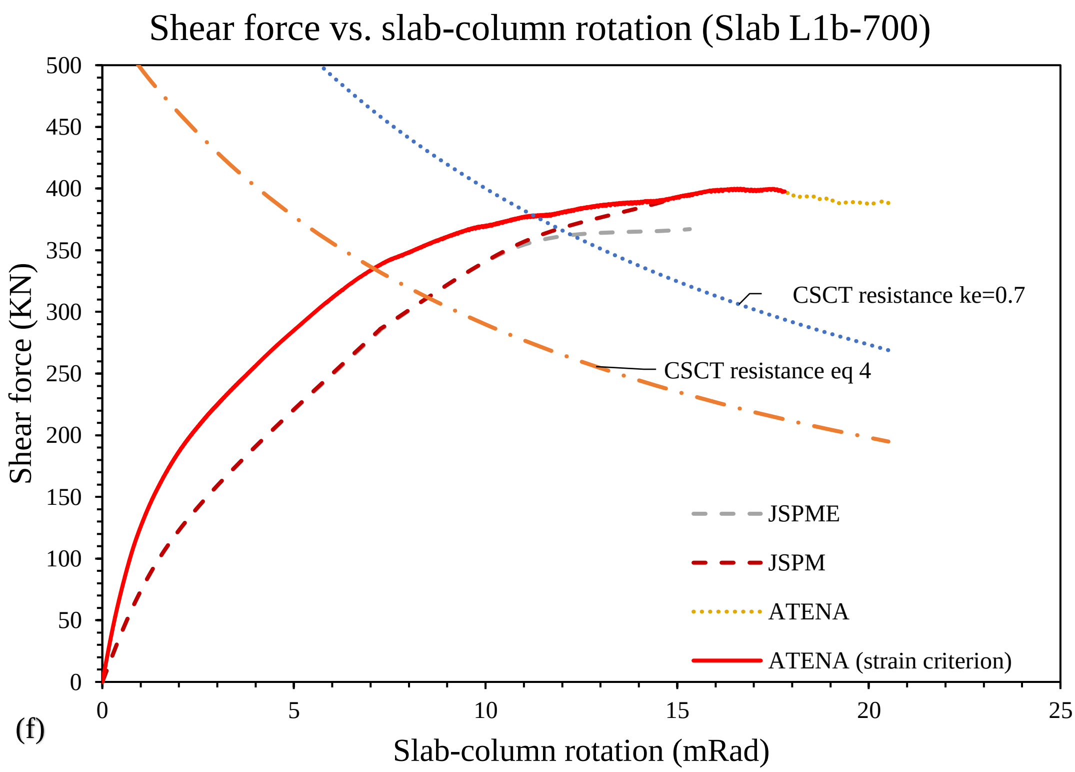

Figure 8: Load-displacement response of specimens a) XXX and b) HXXX of EL-Salakawy et al.[14], c) L2 of Albuquerque et al. [13], d) L1-500, e) L1-700 and f) L1b-700

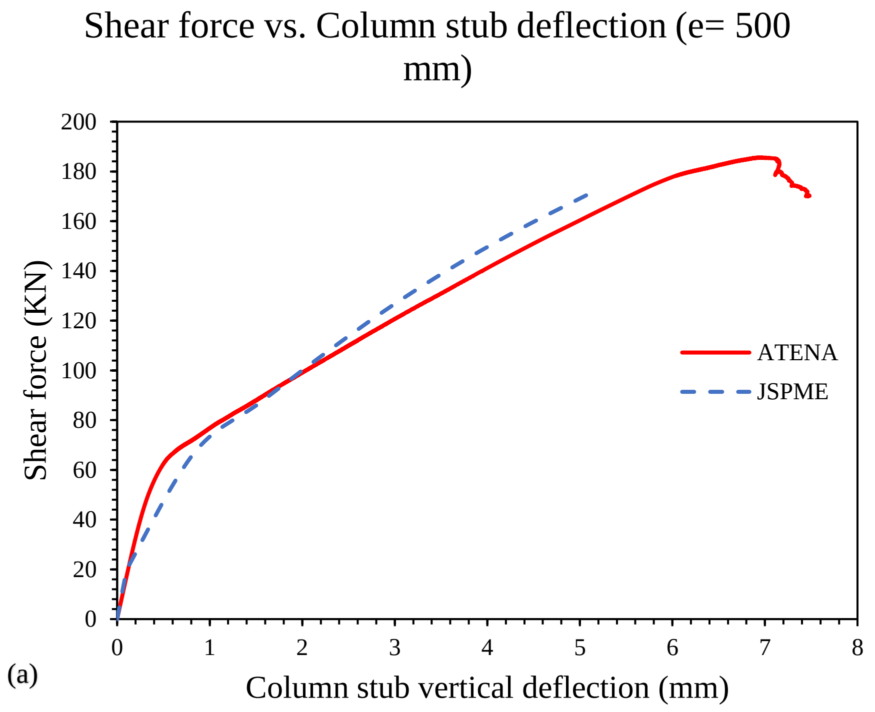

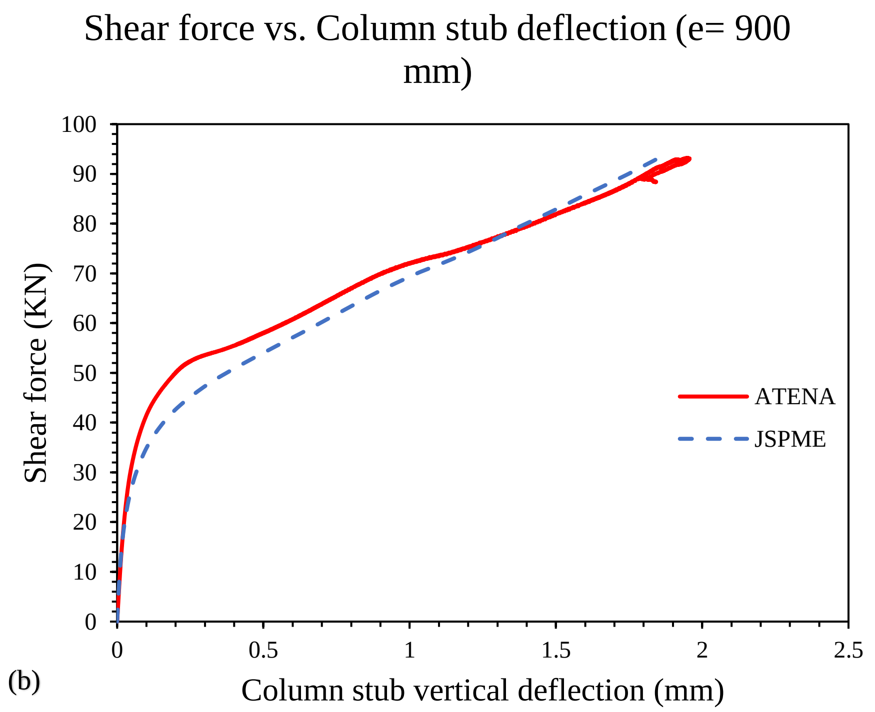

Figure 9: Load-deflection response for slabs XXX [14] 500 x 250 mm (a) e= 500 mm and (b) e= 900 mm

4.1.3 Study of JSPME shear force distribution around control perimeter

Figure 10 shows the influence of loading level on the JSPME joint shear force distribution for HXXX [14] with k_{inc}= 1e12 N/mm. For comparison, the shear force distributions obtained with ATENA and linear elastic analysis with shell elements are also shown at the ATENA failure load (V_{ATENA}). Shear force distributions are shown for half the control perimeter. JSPME shear force distributions are shown at i) V_{ATENA} and ii) the experimental failure load (V_{TEST}) which corresponds to the JSPME failure load of $1.15V_{ATENA}$ (failure of central joint). The JSPME shear force distribution at V_{ATENA} is seen to compare reasonably with that obtained with ATENA. As the load is increased from V_{ATENA} to $1.15V_{ATENA}$, shear force reduces in the joints positioned between 200 mm and 450 mm from the slab edge since post failure the joint shear force follows the softening curve of the CSCT. Figure 10 also shows that the reduction of shear force in failing joints is accompanied by an increase in force in non-failing joints. Interestingly, the positive elastic shear force distribution is similar to that obtained with ATENA at failure.

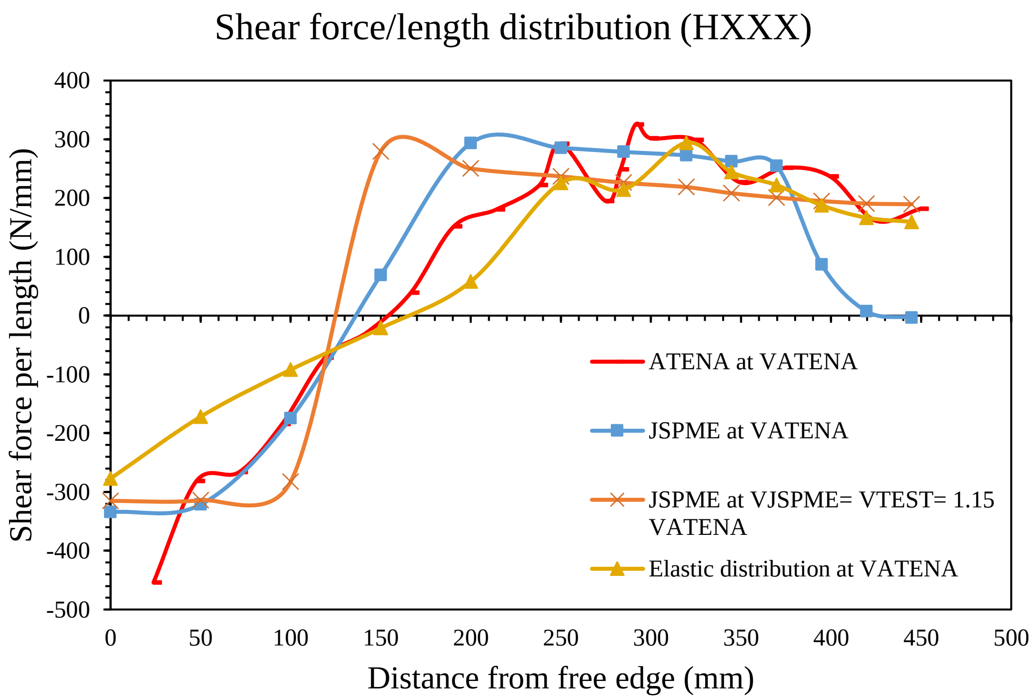

Figure 10: Influence of load on shear force/length distribution for specimen HXXX [14] for k_{inc}= 1e12 N/mm

Figure 11, which is representative of elongated columns, compares shear force/length distributions obtained with ATENA and the JSPME for a 750 mm x 300 mm elongated edge column with loading eccentricity of 700 mm (L1b-700). Results are shown in Figure 11a and 11b at $0.47V_{ATENA}$ and at the JSPME failure load of $0.92V_{ATENA}$, respectively. Failure in the JSPME was assumed to be triggered by failure of the joints located on sides c_1 at 1.5d from the inner column face (see Figure 7). The JSPME joint shear force is zero in the dummy joints positioned along the neglected parts of the control perimeter as indicated in Figure 11a. The shear force in the joint at 150 mm from the free edge in Figure 11b switched direction just before failure at a load of $0.88V_{ATENA}$. This switching of sign of the joint shear force is unrealistic and could be adopted as an alternative failure criterion in the JSPME. The peak joint shear forces in the JSPME at $0.92V_{ATENA}$ are less than given by elastic analysis due to shear redistribution from failing to non-failing joint elements as well as nonlinearity of the shell elements.

The JSPME allows the relative proportions of out of balance moment resisted by torsion, eccentric shear and flexure to be readily determined. For example, at failure of L1b-700, the JSPME predicts 54.3% of the unbalanced moment to be resisted by eccentric shear, 31.7% by flexure and 14.4% by torsion.

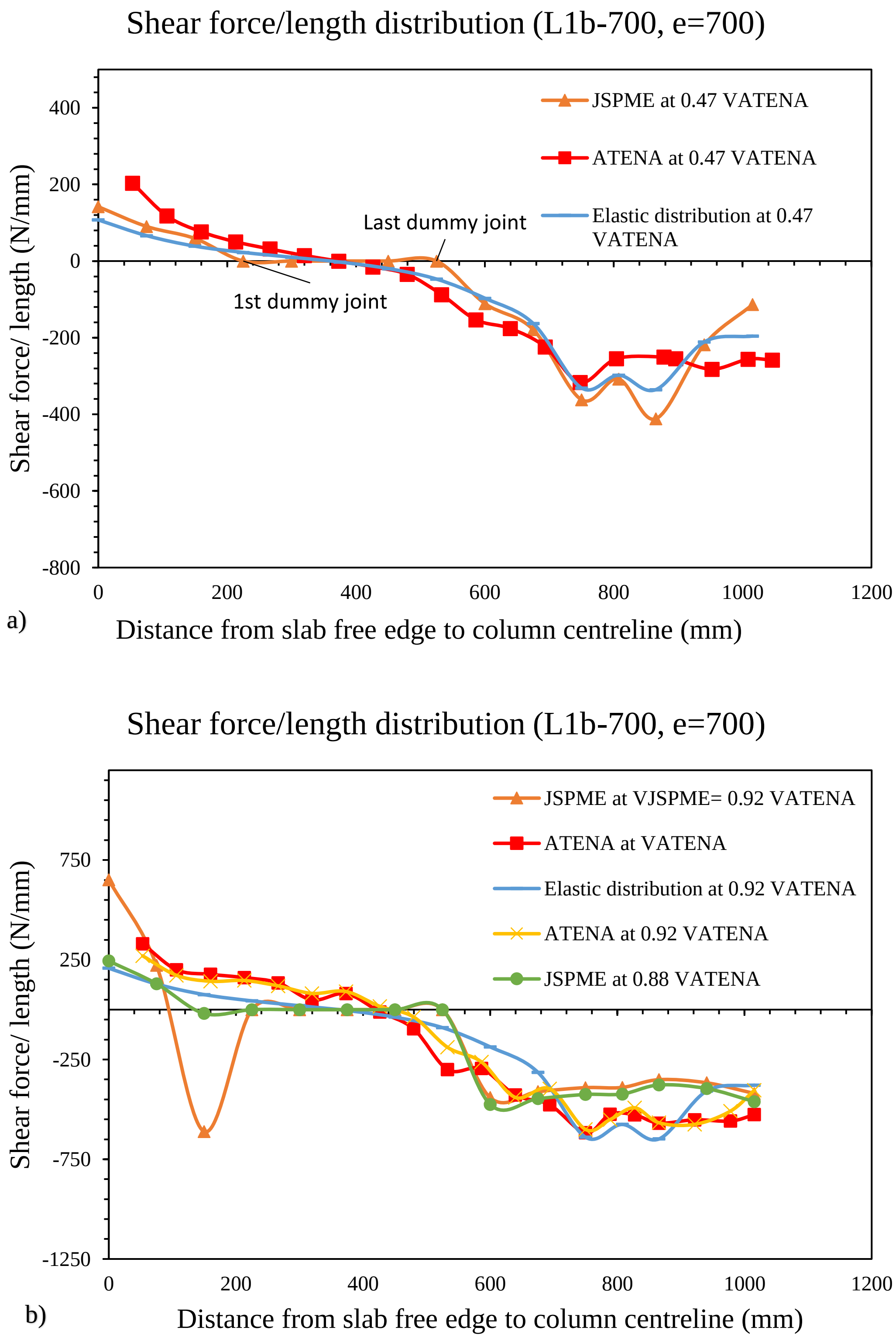

Figure 11: Shear force/length distribution for slab L1b-700 at a) 0.47 Pu ATENA and b) failure from ATENA and the JSPME with k_{inc}=1e12 N/mm and a limit on the torsional strength

4.2. Statistical evaluation of JSPME strength predictions

The JSPME (with k_{inc} = 1e12 N/mm and joint torsional strength limited to T_{cr}) was used to assess the punching resistance of all the edge column specimens in Tables 2 and 4. As previously, failure was assumed to occur at failure of the joints positioned along c_1 at the lesser of $0.5c_1$ and 1.5d from the inner column face. Tables 5 and 6 summarise the failure loads obtained from the JSPME as well as ATENA for experimentally tested and virtual slabs respectively. The predictions of the JSPME and ATENA agree well apart for elongated columns with large loading eccentricities where the JSPME is more conservative. Since test data are not available for these cases, it is unknown which of the JSPME or ATENA predictions are most realistic.

Table 5: Test results and JSPME predictions for experimentally tested slabs

Slab	Column dimensions (mm x mm)	$\rho^{\#}$ %	M_{col}/V (mm)	V_{TEST} (KN)	$V_{flex\ col\ face}^{\dagger}$ (KN)	V_{TEST}/V_{ATENA}	V_{TEST}/V_{JSPME}
L2	300 x 300	1.24	0	315	858	0.99	0.93
L1	300 x 300	0.96	300	308	559	0.89	0.81
XXX	250 x 250	0.79	300	125	124	1.06	1.03
HXXX	250 x 250	0.79	660	69	51	1.13	1.00
S1 end 1	300 x 300	0.56	Varies	282	346	1.12	1.08
S2 end 1	300 x 300	0.56	Varies	256	283	0.99	0.98
S2 end 2	300 x 300	0.56	Varies	285	310	1.08	1.10
S4 end 1	300 x 300	0.66	Varies	289	329	1.07	1.09
S4 end 2	300 x 300	0.45	Varies	281	251	1.08	1.11
				Mean		1.04	1.01
				Standard deviation		0.076	0.098

Notes: # $\rho = \sqrt{\rho_l . \rho_t}$, in which ρ_l and ρ_t are the longitudinal (normal to slab edge) and transverse (parallel to slab edge) flexural reinforcement ratios respectively, † shear force corresponding to flexural failure at column face calculated from equilibrium with tension reinforcement within width of $b_e = 2c_1 + c_2$ (see Figure 7) using eccentricity at end of test.

Table 6: ATENA and JSPME predictions for virtual slabs

Slab	Column dimensions (mm x mm)	$\rho^{\#}$ %	M_{col}/V (mm)	V_{ATENA} (KN)	$V_{flex\ col\ face}^{**}$ (KN)	V_{JSPME} (KN)	V_{JSPME} / V_{ATENA}
L1-500*	300 x 300	1.36	500	301.3	444.6	294.4	0.98
L1-700	300 x 300	2.35	700	270	391.1	267.1	0.99
L1a-500	600 x 300	0.96	500	418.4	607.6	442.2	1.06
L1a-700	600 x 300	1.36	700	335.1	565.1	299.6	0.89
L1a-1000*	600 x 300	1.36	1000	235	322.9	184	0.78
L1b-500	750 x 300	0.96	500	459.1	1122.5	494.7	1.08
L1b-700	750 x 300	1.36	700	399.8	803.9	367.1	0.92
L1b-900*	750 x 300	1.36	900	306	497.6	253.7	0.83
L1b-1200	750 x 300	1.36	1200	226.1	316.7	162.5	0.72
L1c-600	1000 x 300	1.92	600	518.6	2687.1	520.6	1.00
L1c-800	1000 x 300	1.92	800	443	895.7	404	0.91
L1c-1000	1000 x 300	1.92	1000	383.2	537.4	282.6	0.74
L1c-1200	1000 x 300	1.36	1200	252.9	383.9	203.9	0.81
XXX 250 x 250	250 x 250	0.79	203	146.4	204.1	142.2	0.97
			230	148.8	173.1	141.7	0.95
			327	112.2	112.0	103.4	0.92
			394	95.9	90.0	90	0.94
			431	87.7	81.2	85.3	0.97
			486	78.5	70.9	80.1	1.02
			504	76.1	68.1	78.3	1.03
			605	64.1	55.7	68.4	1.07
XXX 500 x 250	500 x 250	1.58	500	185.6	214	170.7	0.92
		1.12	700	127.9	151	128.6	1.00
		1.12	800	108.9	132	101.1	0.93
		1.12	900	93.2	117	93.9	1.01
					Mean		0.93
					Standard deviation		0.098

*Notes:# $\rho = \sqrt{\rho_l . \rho_t}$, in which ρ_l and ρ_t are the longitudinal (normal to slab edge) and transverse (parallel to slab edge) flexural reinforcement ratios respectively, * Strain criterion was used to assess the failure load in this slab, ** shear force corresponding to flexural failure at column face calculated from equilibrium with tension reinforcement within width of $b_e = 2c_1 + c_2$ (see Figure 7).*

5. Comparisons with CSCT and EC2 (2004)

This section compares the predicted influences of column elongation and loading eccentricity on punching resistance according to ATENA, the JSPME, EC2 [30] and the CSCT [7] with the shear resisting control perimeter calculated in accordance with the recommendations of MC2010 [12] which in the presence of loading eccentricities reduces the design shear resistance by a multiple k_e given by:

$$k_e = \frac{1}{(1+\frac{e_u}{b_u})} \tag{4}$$

where e_u is the eccentricity of the column reaction with respect to the centroid of the considered control perimeter, and b_u is the diameter of a circle that has the same enclosed area as the considered control perimeter. Alternatively, in cases where adjacent spans do not differ by more than 25% in length, k_e can be taken as 0.9, 0.7 and 0.65 for interior, edge and corner columns respectively. For columns with side length greater than 3d, MC2010 uses the reduced control perimeter shown in Figure 7b which was also used to calculate b_u.

The CSCT punching resistances were calculated in terms of the maximum relative slab column rotation using the mean CSCT failure criterion of Muttoni [7] (see equation 2) but are depicted MC2010 as it was used to calculate the shear resisting perimeter. In MC2010, the punching resistance is found from the intersection of the load rotation and resistance curves as shown in Figures 8c) to f) which show resistance curves calculated with k_e from equation 4 and k_e = 0.7. Rotations were extracted from the NLFEA with ATENA using 3D solid elements which corresponds to MC2010 Level of Approximation IV (LoA IV). This was done since the ADAPTIC load displacement responses without joint elements tend to be overly stiff as shown in Figures 8d and e. In cases, where the MC2010 failure load was greater than the resistance obtained with ATENA, the load rotation response was obtained by linear extrapolation of the ATENA load rotation curve prior to failure.

In the absence of shear reinforcement, EC2 [30] calculates the design punching shear resistance as:

$$v_c = 0.18(100\rho f_{ck})^{\frac{1}{3}}(1 + (200/d)^{0.5})/\gamma_c \tag{5}$$

where $\rho = \left(\rho_{xl}\rho_{yl}\right)^{0.5} \leq 0.02$ in which ρ_{xl} and ρ_{yl} are the flexural tension reinforcement ratios $\frac{A_{sl}}{bd}$ within a slab width equal to the column width plus 3d to each side. f_{ck} is the characteristic concrete cylinder strength, d is the average effective depth of the tension reinforcement and γ_c is the partial factor for concrete which equals 1.5 for design but 1 here. The term $1 + (200/d)^{0.5}$ is limited to a maximum of 2.

EC2 [30] calculates the design shear stress, which for slabs without shear reinforcement should not exceed v_c from (5) as:

$$v = \beta\frac{V}{u_1 d} \tag{6}$$

where V is the design shear force, u_1 is the length of a control perimeter with rounded corners at 2d from the column face and d is the mean effective depth of the tension reinforcement. The coefficient β accounts for eccentric shear and for edge columns with eccentricity perpendicular to the slab edge can either be taken as 1.4 or calculated as u_1/u_1^* where u_1^* is the reduced perimeter shown in Figure 12 over which shear is assumed to be uniformly distributed. EC2 requires reinforcement perpendicular to the slab edge required to transmit bending moment from the slab to the column to be placed in a width centred on the column of c_2+y where y is the perpendicular distance from the inner column face to the slab edge. However, it is common UK practice [31,32] to provide flexural reinforcement within

$b_e=c_2+2y$. Annex I of EC2, which is informative, limits the maximum moment that can be transferred to edge or corner moments to $M_{tmax} = 0.255(c_2 + y)f_{ck}d_n^2/\gamma_c$ (where d_n is the effective depth of top reinforcement normal to the slab edge and γ_c = 1.5 for design but 1 here). The EC2 [30] failure load is assumed to be limited by the most critical of i) punching failure and ii) flexural failure of the reinforcement within $b_e=c_2+2y$ at the column face (M_{rflex}) both with and without the limit on M_{tmax}. Shear resistances corresponding to M_{rflex} are listed in Tables 5 and 6.

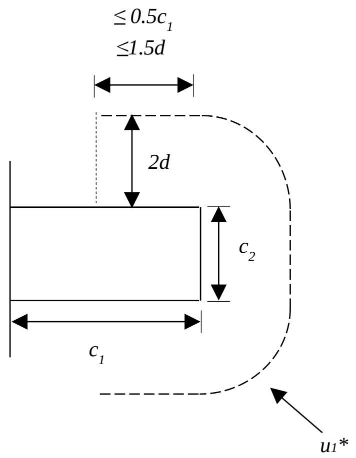

Figure 12: Adopted effective perimeter for EC2 (2004) u1*

Figure 13 compares the punching resistances obtained with ATENA, the JSPME, MC2010 and EC2 (with $\beta = u_1/u_1*$) for slabs XXX and HXXX of EL-Salakawy et al. [14] as well as the virtual slabs in Table 4 with similar geometry (depicted XXX 250 x 250 mm and XXX 500 x 250 mm). Similarly, Figures 14 a to d compare resistances for slabs L1 and L2 of Albuquerque et al. [13] and the virtual slabs derived from them (see Table 4) with column sizes of 300 x 300 mm, 600 x 300 mm, 750 x 300 mm and 1000 x 300 mm respectively. All strengths are calculated with material partial factors of 1.0. EC2 strengths in Figures 13 and 14 are limited by either M_{rflex} (depicted "Mrflex") or the least of M_{rflex} and M_{tmax} (depicted "Mtmax").

The JSPME predictions generally agree well with ATENA, and test results where available, but for virtual specimens based on slab L1 [13] become progressively more conservative with increasing loading eccentricity. Figure 13 shows that at larger eccentricities MC2010 with k_e = 0.7 gives higher punching resistances than ATENA for virtual specimens based on XXX [14]. However, as shown in Figure 14, adopting k_e = 0.7 gives similar punching resistances to the JSPME for virtual specimens with elongated columns based on L1 [13]. The MC2010 strength predictions with k_e from equation (4) follow the general trend of the ATENA results well but with the exception of XXX 250x250 (see Figure 13a) are conservative in comparison. Overall, the MC2010 LoA IV predictions with k_e = 0.7 compare better with the ATENA predictions than those obtained with k_e from equation 4 of MC2010 which tend to be conservative as found in [16]. As shown in Figures 8c to 8f, the JSPME gives significantly larger rotations at punching failure than MC2010 LoA IV which is potentially beneficial for assessment of punching at edge columns of continuous slabs. The JSPME also has the advantage that the punching resistance is determined directly by the NLFEA rather than through post processing as done in MC2010 LoA IV.

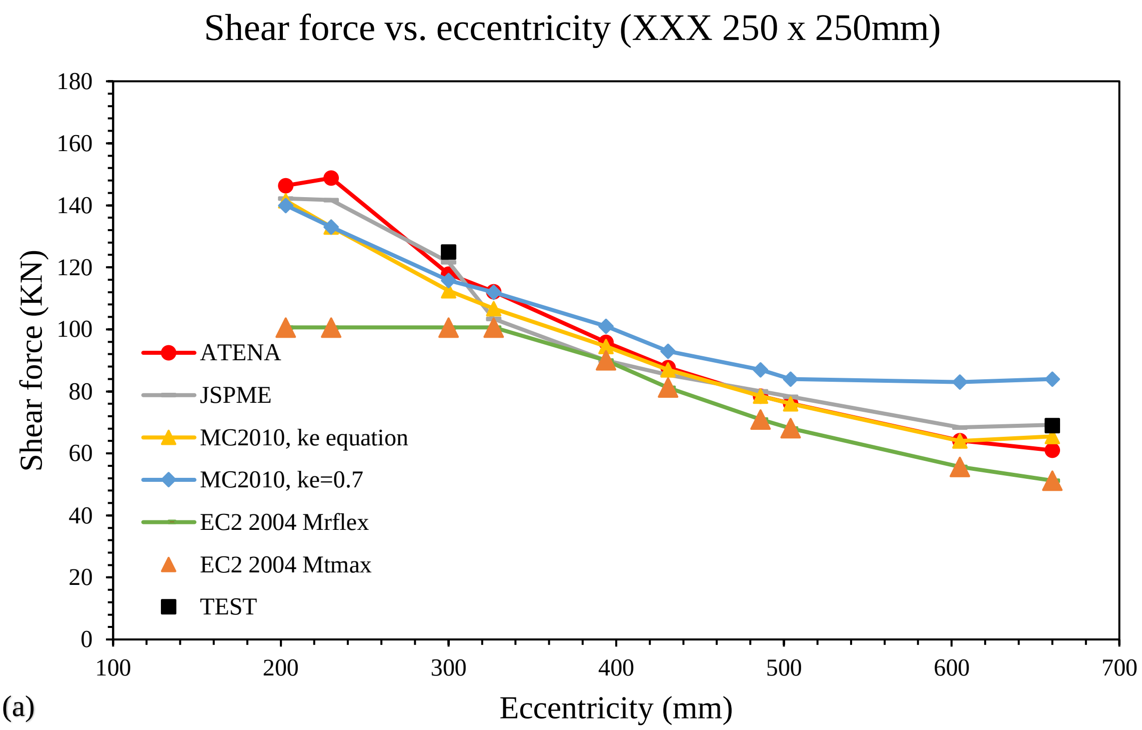

(a)

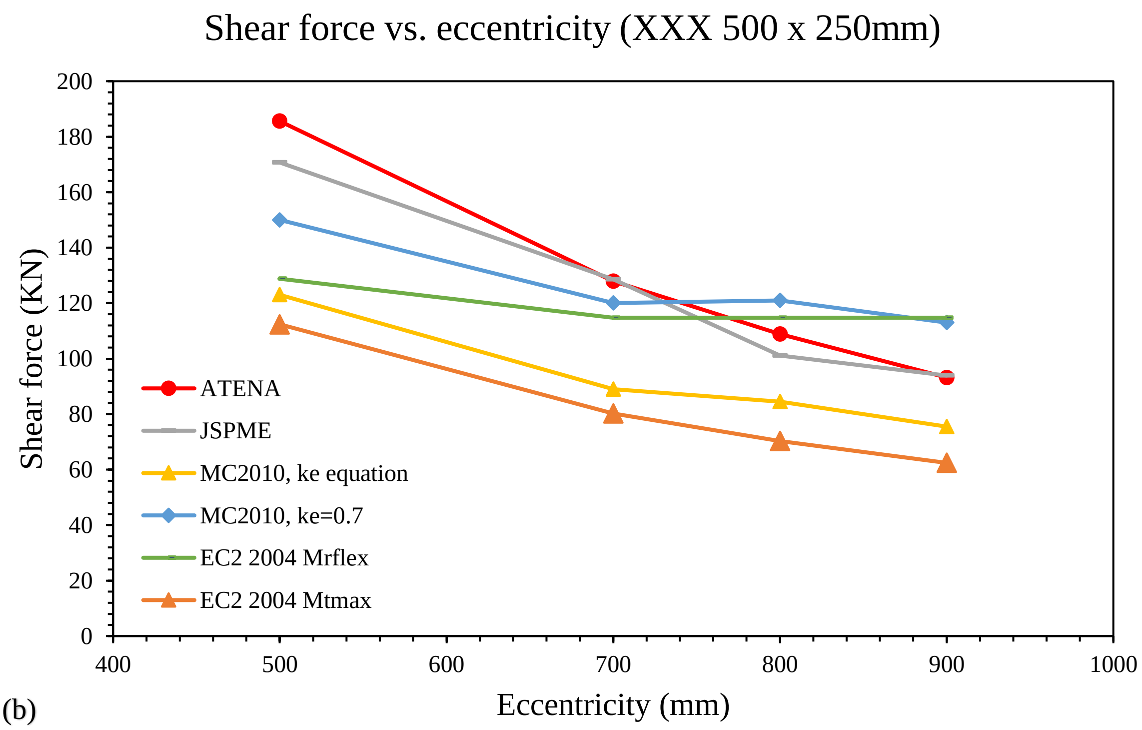

(b)

Figure 13: Shear predictions for EL-Salakawy et al. [14] test set-up slabs supported on a) XXX 250 x 250 mm and b) XXX 500 x 250 mm columns

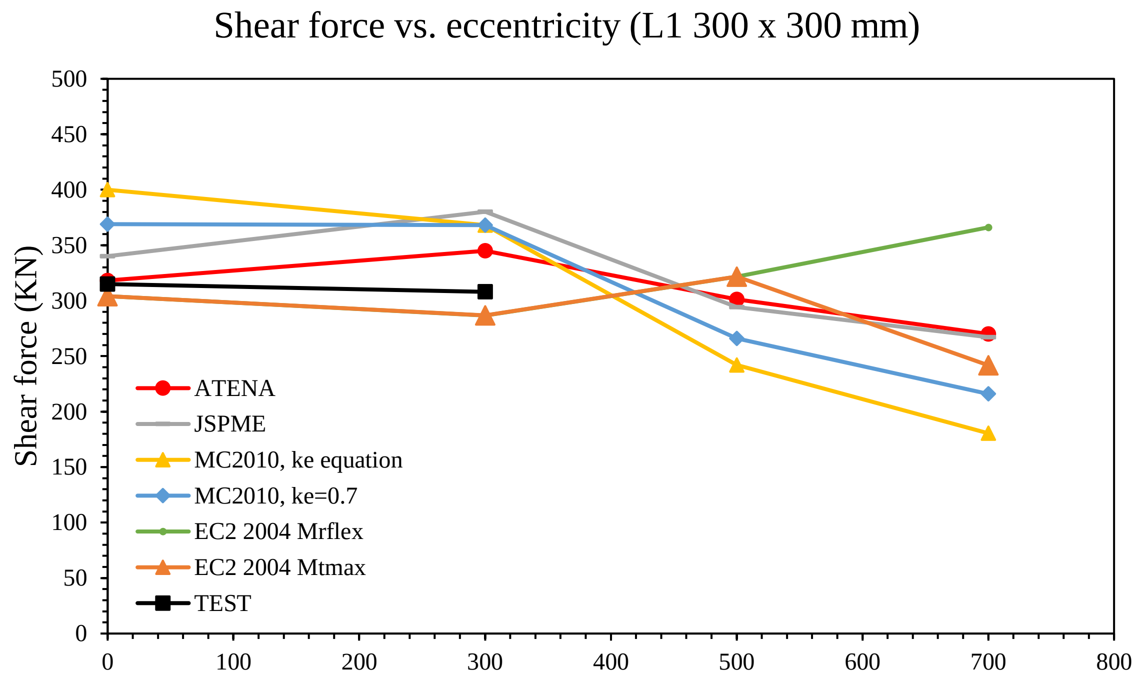

Shear force vs. eccentricity (L1 300 x 300 mm)
Shear force (KN)
Eccentricity (mm)
ATENA
JSPME
MC2010, ke equation
MC2010, ke=0.7
EC2 2004 Mrflex
EC2 2004 Mtmax
TEST
0
50
100
150
200
250
300
350
400
450
500
0
100
200
300
400
500
600
700
800

(a)

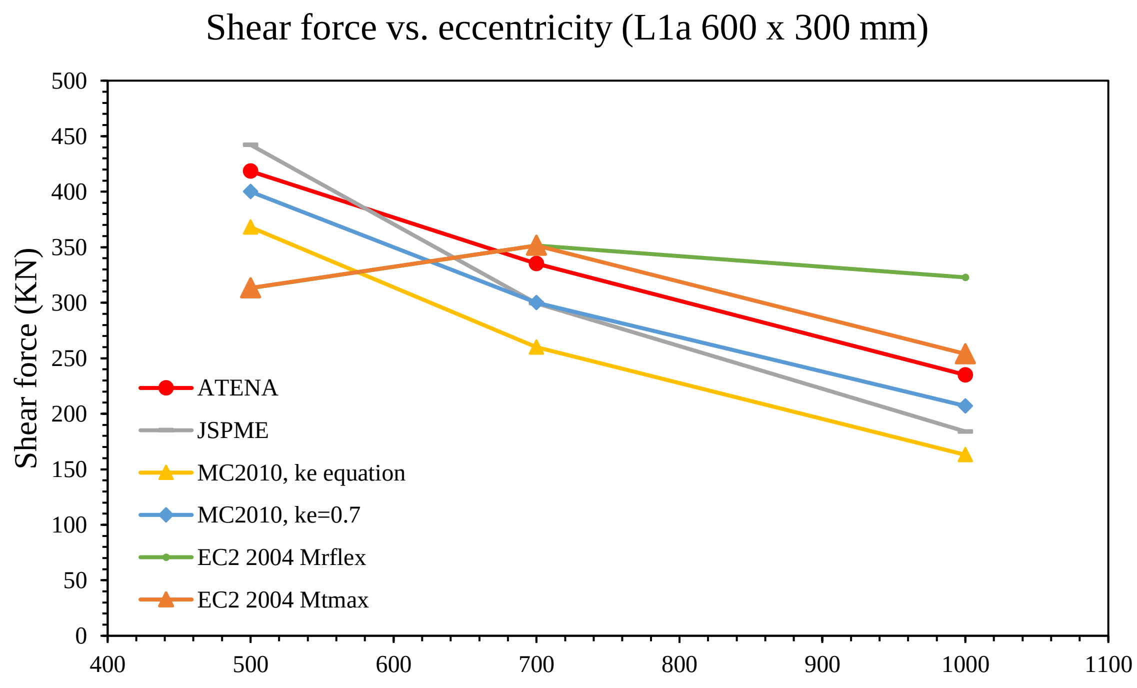

Shear force vs. eccentricity (L1a 600 x 300 mm)
Shear force (KN)
Eccentricity (mm)
ATENA
JSPME
MC2010, ke equation
MC2010, ke=0.7
EC2 2004 Mrflex
EC2 2004 Mtmax
0
50
100
150
200
250
300
350
400
450
500
400
500
600
700
800
900
1000
1100

(b)

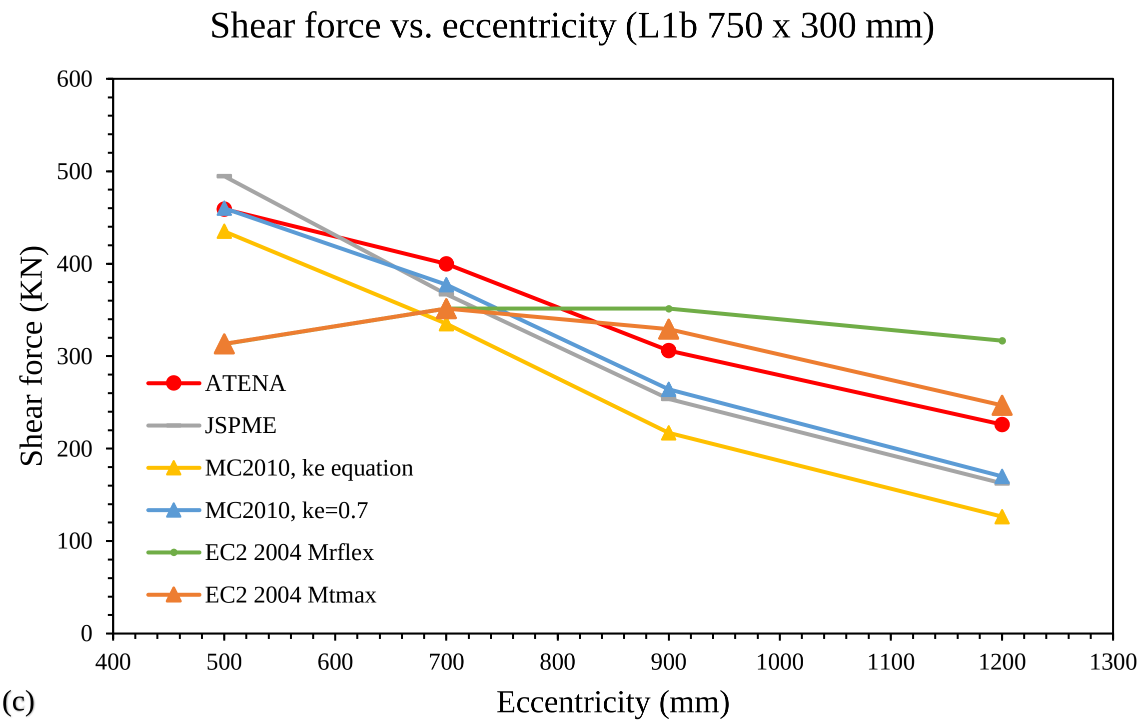

(c)

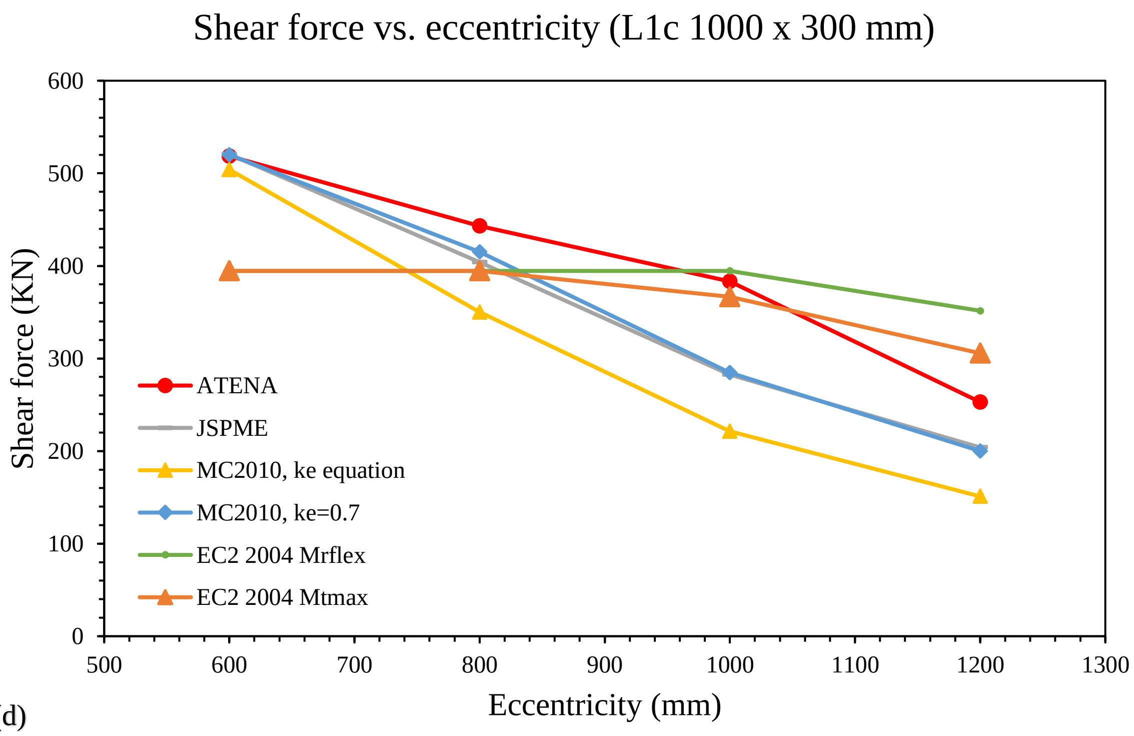

(d)

Figure 14: Shear predictions for Albuquerque et al. [13] test set-up slabs supported on a) 300 x 300 mm, b) 600 x 300 mm, c) 750 x 300 mm and d) 1000 x 300 mm columns

At larger eccentricities, the EC2 [30] predictions are limited by either M_{rflex} or M_{tmax} with strengths overestimated without the introduction of M_{tmax} from Annex I of the code which is only informative. Whilst seemingly necessary for safe prediction of edge column punching resistance, the M_{tmax} limit can be overly conservative as shown in Figure 13b. Overall the trend of the ATENA and experimental punching resistances is best captured by the JSPME followed by MC2010 with k_e = 0.7 as indicated in the statistics of Table 7. Use of MC2010 with k_e from equation 4 is overly conservative bearing in mind that punching resistances in Figures 13 and 14 were calculated with Muttoni's [7] mean strength criterion rather than the characteristic strength formula of MC2010.

Figures 13 and 14 show that punching resistance reduces with increasing eccentricity relative to the column centre line (M_{col}/V). This raises the question of whether increasing the column side length c_1 normal to the slab edge in flat slab buildings increases or decreases punching resistance. This is explored in Figure 15 which shows the influence of loading eccentricity (M_{col}/V) on the punching resistance of various virtual slabs based on the Albuquerque et al. [13] test set up. Also shown in Figure 15 are loading eccentricities calculated with elastic analysis for each column size for a flat slab of thickness 180 mm (i.e. same as [13]) having square bays of span 5.4 m measured between column centrelines. These results, along with corresponding ones in which the elastic edge column moment is redistributed downwards by 20%, suggest that punching resistance increases with increasing column side length c_1 despite i) the length of the MC2010 control perimeter (Figure 7b) remaining constant for column sides greater than 3d = 441 mm and ii) the loading eccentricity M_{col}/V increasing with c_1 due to increased column flexural rigidity. Only in the case of the 1000×300 mm^2 column is the increase in punching resistance with side length c_1 attributable in part to an increase in reinforcement ratio $\rho = \sqrt{\rho_l . \rho_t}$.

Table 7: Statistical analysis of $V_{calculated}/V_{ATENA}$ for virtual slabs in Table 4

Calculated/ATENA	JSPME	MC2010 k_e=0.7	MC2010 k_e equation 4	EC2 (2004)
Mean	0.94	0.96	0.82	0.88
Standard deviation	0.09	0.13	0.14	0.16
COV	0.10	0.14	0.17	0.18

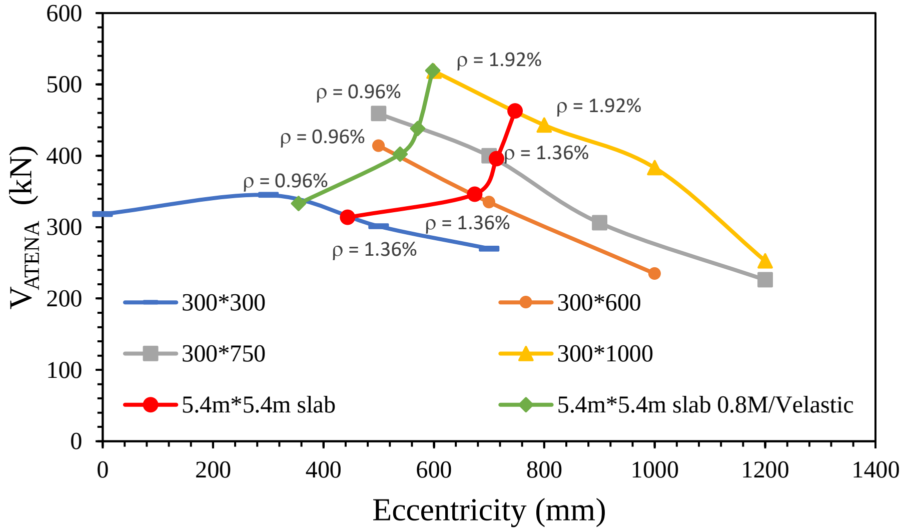

Figure 15: Influence of increasing column side length c_1 on punching resistance predicted by ATENA at edge column of 180 mm thick flat slab spanning 5.4 m between columns.

A further question arises as to whether the shear force distributions around the control perimeter are similar for uniformly loaded flat slabs and the virtual slabs considered in the parametric studies. This is examined for two representative examples in Figure 16. The similarity of the normalised shear force distributions obtained for the full scale and virtual slabs derived from [13] suggests that the results in Figures 13 and 14 are generally applicable.

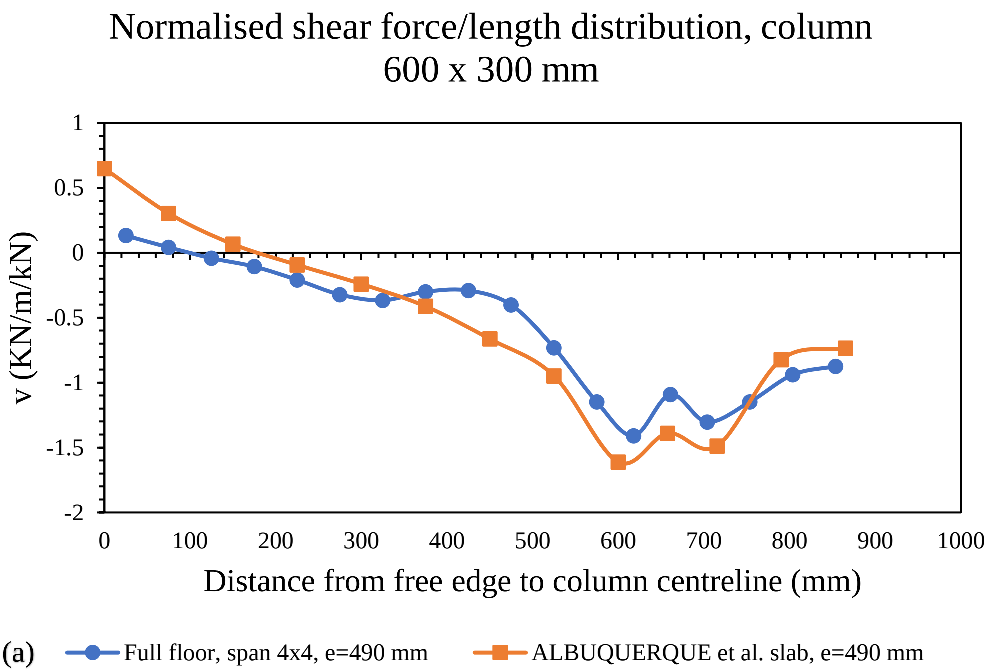

(a)

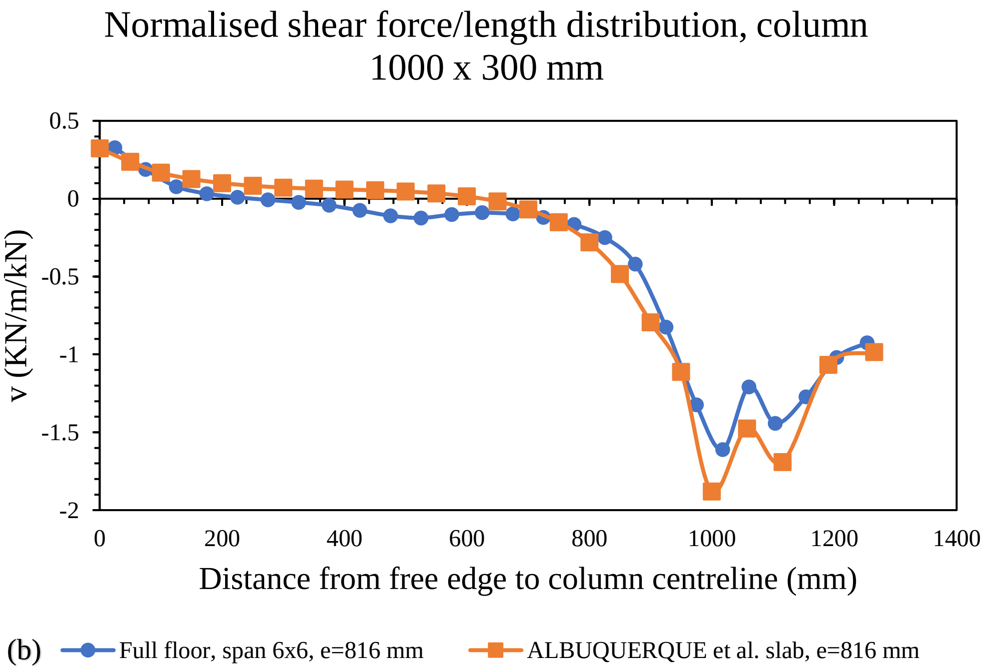

(b)

Figure 16: Comparison of elastic shear force distributions around punching control perimeter for flat slab and virtual slabs based on [13] for a) 600*300 mm column and b) 1000*300 mm column.

6. Punching shear failure in continuous edge slab-column connections

The loading eccentricity was constant in all the specimens considered in this paper except for the continuous slabs of Regan [15] which are most representative of flat slabs. The influence of slab continuity was investigated by modelling slabs S1, S2 and S4 of Regan with ATENA. Taking advantage of symmetry, only half of the slab was modelled (see Figure 5). Figure 17 shows the variation in loading eccentricity with column reaction for a) S1 end 1, b) S2 end 1, c) S2 end 2, d) S4 end 1 and e) S4 end 2 as measured in the test as well as ATENA. In all cases, both the calculated and measured loading eccentricity are seen to reduce as the load is increased to failure. The difference in initial eccentricity in the tests and NLFEA is due to differences in loading procedure. In the tests, equal and opposite horizontal forces were applied to the column at the end under test 'so as to keep the column free of rotation' [15] but in the NLFEA, the columns were restrained laterally at each end throughout the analysis. In all cases, the measured and predicted loading eccentricity drops below the elastic value as the load is increased to failure. This behaviour is considered representative of edge columns in flat slab buildings and implies that it is overly conservative to relate punching strength at edge columns to the elastic eccentricity as done in design codes like MC2010 but not EC2 [30]. In Figure 17, the ATENA eccentricities reduce from the elastic value of 0.73 m to local minima of 0.57 m and 0.59 m. Subsequently, the eccentricity slightly rises prior to dropping again near failure. The initial drop in eccentricity is caused by localised cracking in the slab around the column, and cracking of the column, which causes moment to be redistributed to the span. Subsequently, cracking in the span causes moment to be redistributed back to the column causing the calculated eccentricity to rise above the local minimum. The final drop in eccentricity is associated with the column transfer moment levelling off, due in part to yielding of hogging reinforcement at the column face, and finally reducing.

The influence on punching resistance of eccentricity reducing during loading was studied further for slabs XXX (e= 300 mm) and HXXX (e= 660 mm) of EL-Salakawy et al. [14]. The specimens were modelled using 3D solid elements in ATENA as well as the JSPME. Load was initially applied at a constant loading eccentricity after which the load was increased at continually reducing eccentricity. The results are presented in Figure 18 and Table 8 which also shows failure loads calculated with constant eccentricity equal to the final eccentricity reached in the analyses with varying eccentricity. As shown in Table 8, the slabs with constant eccentricities are predicted to fail, especially by ATENA, at very similar loads to the corresponding slabs loaded with varying eccentricity. This implies that the punching resistance depends on the loading eccentricity at failure rather than the initial elastic loading eccentricity. The benefit of accounting for the reduced eccentricity at failure is illustrated in Figure 15 where punching resistances are shown for a 5.4 m square flat slab without and with 20% moment redistribution at the edge columns.

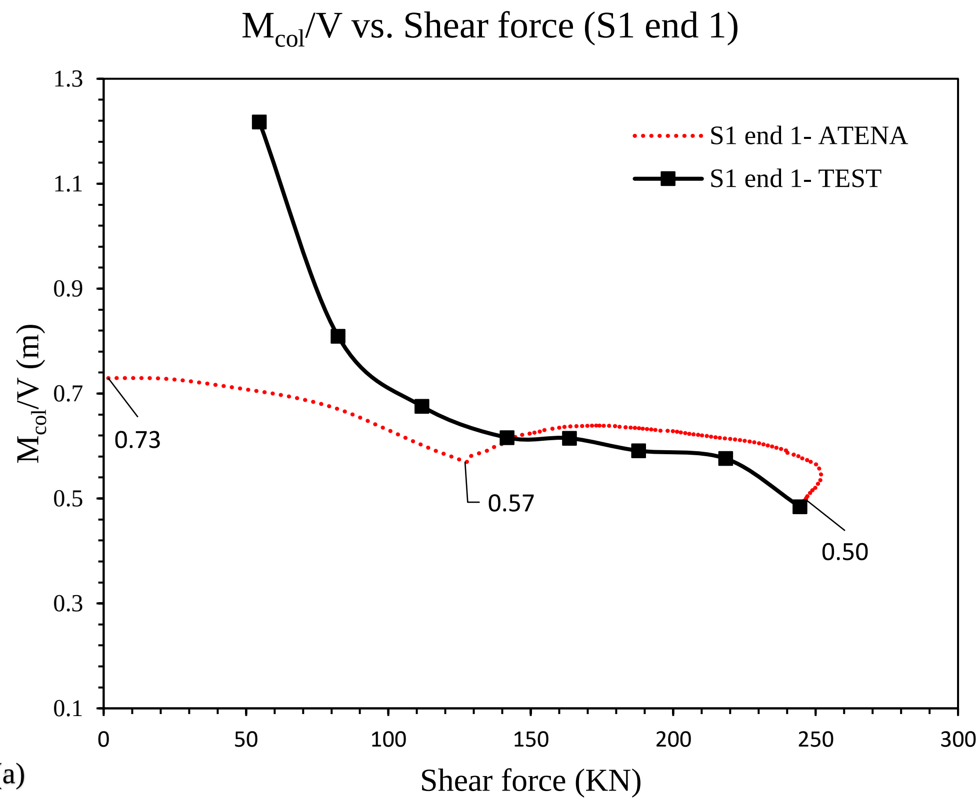

M_{col}/V vs. Shear force (S1 end 1)
S1 end 1- ATENA
S1 end 1- TEST
0.73
0.57
0.50
M_{col}/V (m)
Shear force (KN)
1.3
1.1
0.9
0.7
0.5
0.3
0.1
0
50
100
150
200
250
300

(a)

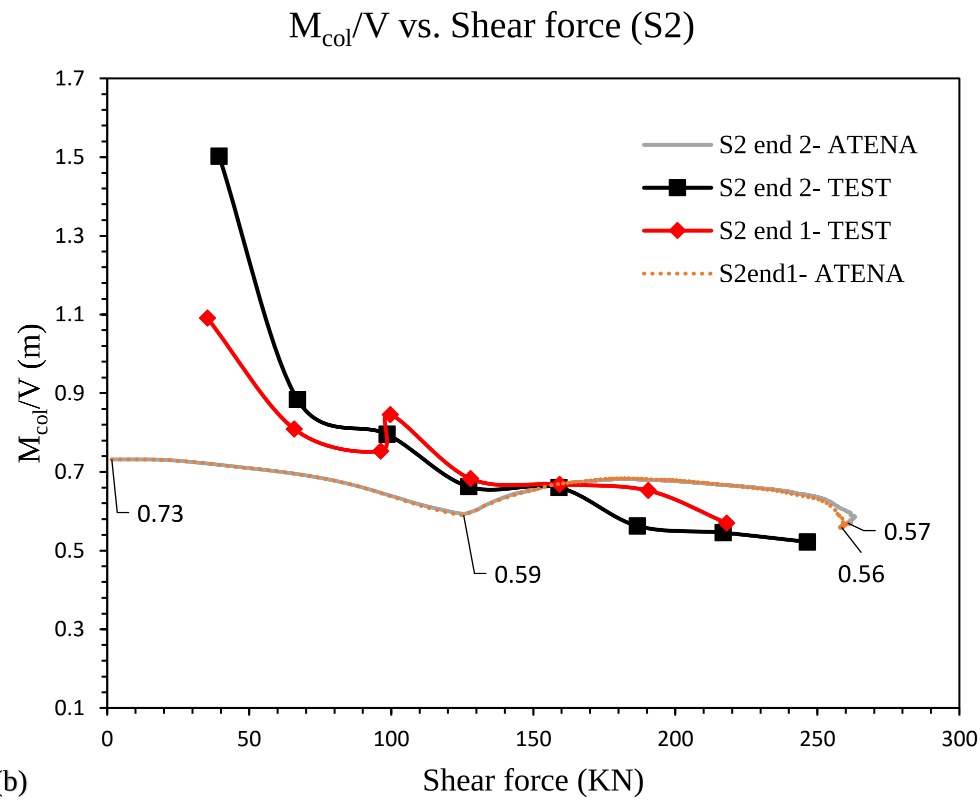

M_{col}/V vs. Shear force (S2)
S2 end 2- ATENA
S2 end 2- TEST
S2 end 1- TEST
S2end1- ATENA
0.73
0.59
0.57
0.56
M_{col}/V (m)
Shear force (KN)
1.7
1.5
1.3
1.1
0.9
0.7
0.5
0.3
0.1
0
50
100
150
200
250
300

(b)

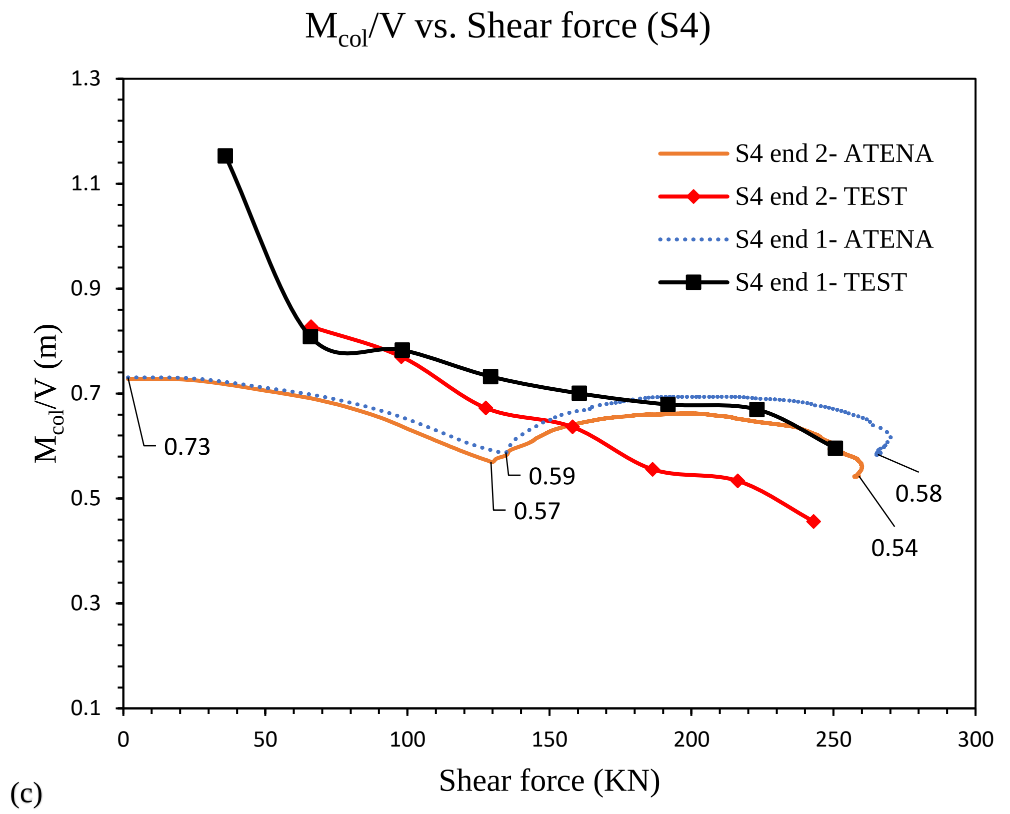

Figure 17: Measured and predicted loading eccentricity vs. column reaction for Regan [15] slabs a) S1 end 1, b) S2 end 1, c) S2 end 2, d) S4 end 1, S4 end 2.

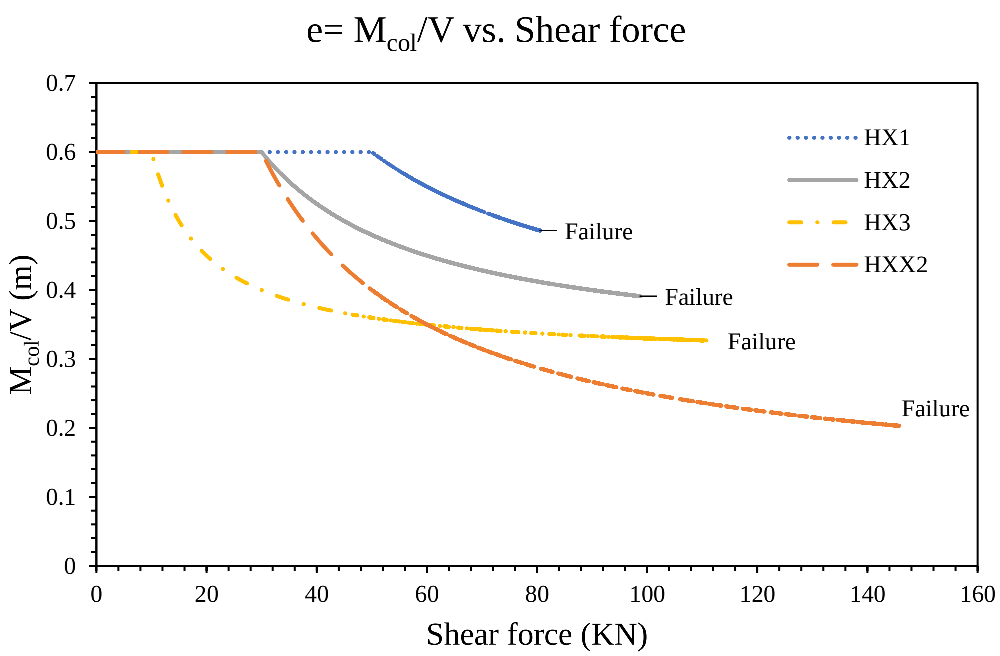

Figure 18: Load path for analyses of specimens in Table 8 with varying loading

Table 8: Parametric study of virtual slabs based on XXX [14] with variable eccentricity (M_{col}/V)

Slab notation	Eccentricity = M_{col}/V (mm) up to failure	V_{JSPME} (KN)	V_{ATENA} (KN)	% Difference
HX1	600 to **486**	84.2	80.6	4.5%
HX2	600 to **394**	91.9	98.7	-6.9%
HX3	600 to **327**	101.6	111.9	-9.2%
HXX2	600 to **203**	131.2	146.1	-10.1%
HX1- **486**	486	80.1	78.5	2%
HX2- **394**	394	90	95.9	-6.2%
HX3- **327**	327	103.4	112.2	-7.8%
HXX2- **203**	203	142.2	146.4	-2.9%

Note: Eccentricity at failure is highlighted in bold

7. Conclusions

This paper extends the internal column joint shell punching model (JSPM) of [6] to the analysis of edge slab-column connections without shear reinforcement. In this model, punching failure is modelled with 3D joint elements that are inserted between nonlinear shell elements around the punching control perimeter which is located at 0.5d from the column face. The resulting model, depicted JSPME, is validated for both isolated and continuous edge column punching specimens with different column aspect ratios and loading eccentricities. The influence of column elongation on punching resistance at edge columns has not been investigated experimentally. Consequently, the validation of the JSPME for elongated edge columns relies on the assessment of virtual slabs with NLFEA using 3D solid elements. The virtual specimens were derived by extending the slab and column of specimens tested by [13] and [14] backwards to form elongated edge columns of varying cross-section. A range of eccentricities obtained from elastic analysis of representative flat slab buildings was investigated for both test set-ups.

Modifications to the JSPM of Setiawan et al. [6] include increasing the out-of-plane joint shear stiffness and limiting the joint torsional strength. Global punching failure is triggered by failure of the joints located along the sides of the control perimeter perpendicular to the slab edge at the least of $0.5c_1$ and 1.5d from the inner column face. These modifications are found to predict punching resistance well when compared to test results and 3D solid element simulations of virtual slabs. The JSPME also gives similar distributions of shear force around the punching control perimeter to NLFEA with ATENA using 3D solid elements. Punching resistances obtained with the JSPME and ATENA are also compared with the predictions of MC2010 LoA IV and EC2. The best MC2010 predictions were obtained using k_e = 0.7 with equation 4 from MC2010 for k_e giving overly conservative results. In the case of EC2, the introduction of the M_{tmax} limit of Annex I (informative) was found necessary to avoid overestimate of punching resistance. The influence of slab continuity on punching resistance is investigated using the continuous edge slab-column connections of Regan [15]. Both the test results and NLFEA show loading eccentricity to reduce below its initial elastic value as loads are increased to failure. Based on these observations, isolated edge slab-columns were modelled with i) gradually decreasing loading eccentricity to simulate the effect of slab continuity and ii) uniform eccentricity equal to the final eccentricity in i). The failure loads obtained with loading scenarios i) and ii) were very similar indicating that punching resistance depends on the final rather than the initial loading eccentricity. Consequently, basing the design shear resistance on the elastic loading eccentricity appears conservative.

8. Acknowledgments

Special thanks to the authors of [6] for providing the Fortran script used in running the JSMP and the JSPME in this paper.

9. Notation

b_0 = shear resisting control perimeter

$b_{0,3d}$ = maximum shear resisting control perimeter according to MC2010

b_u = diameter of a circle that has the same enclosed area of the considered control perimeter

c_1 = column long side

c_2 = column short side

d = average slab effective depth

d_g = maximum aggregate size

E_c = concrete elastic modulus

e_u = eccentricity of the column reaction with respect to the centroid of the considered control perimeter

f_c = concrete compressive strength

f_{ck} = characteristic concrete compressive strength

f_{ct} = concrete tensile strength

h = slab thickness

k = size effect factor in EC2 (2004)

k_{inc} = out-of-plane shear stiffness

k_{red} = an out-of-plane stiffness reduction factor accounting for cracking

k_e = MC2010 reduction factor

l_{si} = spacing of joint i

L = span length

M_{col}: moment transferred from slab to column

ψ_{si} = relative slab column sector rotation for joint i

T_{cr} = concrete cracking strength

u_1: basic control perimeter according to EC2 (2004)

u_1*: reduced basic control perimeter according to EC2 (2004)

V: column reaction (Shear force)

v_c = design punching shear resistance in EC2 (2004)

v = Poisson's ratio taken as 0.2

w_d = critical compressive displacement

β_s = shear retention factor

ρ = flexural reinforcement ratio

ρ_l = longitudinal flexural reinforcement ratio

ρ_t = transverse flexural reinforcement ratio

γ_c = partial factor for concrete = 1.5 according to EC2 (2004)

10. References

[1] Polak, MA. Shell finite element analysis of RC plates supported on columns for punching shear and flexure. *Engineering Computations. 2005;*22(4), 409–28.

[2] Hrynyk, TD., Vecchio FJ. Capturing out-of-plane shear failures in the analysis of reinforced concrete shells. *Journal of Structural Engineering.* 2015;141(12), 04015058

[3] Keyvani, L., Sasani, M., Mirzaei, Y. Compressive membrane action in progressive collapse resistance of RC flat plates. *Engineering Structures.* 2014;59, 554–64.

[4] Liu, J., Tian, Y., Orton, S.L., Said AM. Resistance of flat-plate buildings against progressive collapse. Part I: Modeling of slab-column connections *Journal of Structural Engineering*. 2015;141(12).

[5] Liu, J., Tian, Y., Orton, S.L., Said, A.M. Resistance of flat-plate buildings against progressive collapse. Part II: system response. *Journal of Structural Engineering. 2015;*141(12).

[6] Setiawan, A., Vollum, R.L., Macorini, L., Izzuddin, B. Efficient 3-D modelling of punching shear failure at slab-column connections by means of nonlinear joint elements. *Engineering Structures.* 2019*;* 197.

[7] Muttoni A. Punching shear strength of reinforced concrete slabs without transverse reinforcement. *ACI Structural Journal. 2008;*105 (4), 440-450.

[8] Cervenka, V., Jendele, L., Cervenka, J. *ATENA Program Documentation, Part 1, Theory.* Cervenka Consulting, Prague; 2018. P.334.

[9] Setiawan, A., Vollum, R. L., Macorini, L. Numerical and analytical investigation of internal slab-column connections subject to cyclic loading. *Engineering Structures.* 2019*;*184(1), 535-554

[10] Setiwana, A., Vollum, R.L., Macorini, L., Izzuddin, B. Punching of RC slabs without transverse reinforcement supported on elongated columns. *Structures*. 2020;27, 2048-2068.

[11] Vecchio, F.J., Collins, M.P. The modified compression-field theory for reinforced concrete elements subjected to shear. *ACI Structural Journal*. 1986;83(2), 219–31.

[12] fib (Fédération International du Béton). fib Model Code for concrete structures. 2010. Lausanne, Switzerland: Fédération International du Béton; 2013.

[13] Albuquerque, N. G. B., Melo, G. S., Vollum, R. L. Punching shear strength of flat slab-edge column connections with outward eccentricity of loading. *ACI Structural Journal.* 2016*;*113(5): 1117-1129.

[14] El-Salakawy, E. F., Polak, M. A., Soliman, M. H. Slab-column edge connections subjected to high moments. *Canadian Journal of Civil Engineering.* 1998;25(3): 526-538.

[15] Regan, P.E. Tests of Connections between Flat Slabs and Edge Columns. School of Architecture and Engineering, University of Westminster, London, UK; 1993.

[16] Soares, L. F. S., Vollum, R. L. Influence of continuity on punching resistance at edge columns. *Magazine of Concrete Research.* 2016;68(23), 1225-1239.

[17] Sagaseta, J., Muttoni, A., Ruiz, M., Tassinari, L. Non-axis-symmetrical punching shear around internal columns of RC slabs without transverse reinforcement. *Magazine of Concrete Research.* 2011*;*63(6), 441-457.

[18] Teng, S., Gheong, H. K., Kuang, K. L., Gneg, J. Z. Punching shear strength of slabs with openings and supported on rectangular columns. *ACI Structural Journal.* 2004;101(5), 678-687.

[19] Ferreira, M. D. P. *Punção em lajes lisas de concreto armado com armaduras de cisalhamento e momentos desbalanceados*. PhD Thesis. The University of Brasília; 2010.

[20] Genikomsou, A., Polak, M. Finite element analysis of punching shear of concrete slabs using damaged plasticity model in ABAQUS. *Engineering Structures.* 2015;98: 38-48.

[21] ABAQUS Analysis user's manual 6.12. Providence (RI, USA): Dassault Systems Simulia Corp.; 2012.

[22] Ferreira, M.P., Melo, G.S., Regan, P.E., Vollum, R.L. Punching of reinforced concrete flat slabs with double-headed shear reinforcement. *ACI Structural Journal*. 2014;111(2): 363–374.

[23] Broms, C. E. Tangential strain theory for punching failure of flat slabs. *ACI Structural Journal.* 2016;113(1): 95-104.

[24] Setiawan, A. *Efficient strategy for modelling punching failure in flat slabs.* PhD thesis. Imperial College London; 2019.

[25] Goodchild, C. H., Webster, R. M., Elliott, K. S. *Economic Concrete Frame Elements to Eurocode 2.* Surrey, The Concrete Centre; 2009.

[26] Izzuddin, BA. *Nonlinear Dynamic Analysis of Framed Structures*. PhD Thesis. Imperial College London; 1991.

[27] Soares, L. F. S. *Influence of slab continuity on punching resistance.* PhD thesis. Imperial College London; 2017.

[28] Vollum, R.L., Tay, U.L. Modelling tension stiffening in reinforced concrete with NLFEA. *Concrete*. 2007;41(1): 40–41.

[29] Hsu, T. T. C. Torsion of structural concrete-behavior of reinforced concrete rectangular members. *ACI Special Publication*. 1968;18-08, 261–306.

[30] BSI. BS EN 1992-1-1:2004: Eurocode 2, design of concrete structures – part 1–1: general rules and rules for buildings. London, UK: BSI; 2004.

[31] ISE (The Institution of Structural Engineers). *Standard Method of Detailing Structural Concrete*. The Institution of Structural Engineers, London, UK; 2006.

[32] The Concrete Society. *Guide to the Design and Construction of Reinforced Concrete Flat Slabs*. The Concrete Society, Camberley, UK, Technical Report 64; 2007.